Ultrasonics - Sonochemistry 62 (2020) 104722

Contents lists available at ScienceDirect

Ultrasonics - Sonochemistry

journal homepage: www.elsevier.com/locate/ultson

Power ultrasound and its applications: A state-of-the-art review

Ye Yao[a], Yue Pan[a], Shiqing Liu[b,*]

[a] Institution of Refrigeration & Cryogenics, Shanghai Jiao Tong University, Shanghai 200240, China
[b] Institute of Mathematics and Physics, Zhejiang Normal University, Zhejiang 321004, China

ARTICLE INFO

Keywords:
Ultrasound
High-intensity
Transducer
Magnetostrictive
Piezoelectric
Applications

ABSTRACT

Ultrasonic processing has attracted increasing attention by people because ultrasonic technology may represent a flexible 'green' alternative for energy efficient processes. The major challenges for the power ultrasound application in real situations are the design and development of specific power ultrasonic systems for large-scale operations. Thus, new families of power ultrasonic transducers have been developed in recent years to meet actual needs, and this contributes to the implementation of power ultrasound of application in many fields such as chemical industry, food industry and manufacturing. This paper presents the current state of ultrasonic transducers of magnetostrictiv type and piezoelectric type as well as applications of power ultrasound in various industrial fields including chemical reactions, drying/dehydration, welding, extraction, heat transfer enhancement, de-ice, enhanced oil recovery, droplet atomization, cleaning and fine particle removal. The review paper helps to understand the current development of power ultrasonic technology and its applications in various situations, and induce extended applications of power ultrasound to more and more fields.

1. Introduction

Ultrasound involves generation of acoustic longitudinal waves whose frequencies are higher than the threshold of human auditory detection (normally ≥ 16 kHz). Power ultrasound is the high-intensity application of ultrasonic energy which is usually higher than 0.1 W/cm^2, and its frequency often ranges from 16 to 100 kHz.

Power ultrasound has been widely used in ultrasonic plastic soldering and metal welding, ultrasonic machining, ultrasonic cell disruption, ultrasonic extraction, ultrasonic cutting, ultrasonic drilling and other high intensity ultrasonic applications where high mechanical displacement magnitude is needed, as well as metal forming in solids and cleaning, atomization, emulsification and dispersion, degassing and sonochemical reactions in liquids. In recent years, there has been a renewed interest in ultrasonic processing, particularly in those sectors where the ultrasonic energy may represent a clean and efficient tool, for example in the food industry, the environment, pharmaceuticals, chemicals manufacture, etc. At present, the implementation of new environmentally friendly and energy-saving technologies is one of the main objectives in the improvement of the quality of life. Power ultrasound can be considered to belong to this class of technologies and its successful use in medical therapy has underlined its innovative character.

The potential of power ultrasound involves physical and chemical processes. The physical processes are mainly due to the mechanical effects of the high intensity waves in a medium while the chemical processes are the chemical effects induced by ultrasonic cavitation in liquids. The latter processes are within the field of sonochemistry while the general term for the whole area is sonoprocessing or power ultrasonic processing.

The applications of high-intensity ultrasonic waves are based on the adequate exploitation of the non-linear effects associated with high amplitudes, such as the radiation pressure, streaming, cavitation, dislocation in solids, etc. As a consequence of these effects, a series of mechanisms are activated by the ultrasonic energy, such as heat, agitation, diffusion, interface instabilities, friction, mechanical rupture, chemical reactions, etc. These mechanisms can be employed to produce or to enhance a wide range of processes that depend on the irradiated medium to a large degree. In fact, a typical characteristic of high-intensity ultrasonic waves is their ability to produce different processes in different media in such a way that they seem to have opposite effects at times. For example, power ultrasound is used in liquid suspensions for particle dispersion and in gas suspensions for particle agglomeration. Such apparently contradictory behavior is clearly due to the different

Abbreviations: DEA, discrete energy averaged; GMMs, giant magnetostrictive materials; GMA, giant magnetostrictive actuator; MTRT, magnetostrictive torsional resonant transducer; MPTs, magnetostrictive patch transducers; NDT, nondestructive testing; PZT, piezoelectric ceramic transducer; SH, shear-horizontal; TMM, transfer matrix method

* Corresponding author.
E-mail address: shiqingliu@zjnu.cn (S. Liu).

https://doi.org/10.1016/j.ultsonch.2019.104722
Received 8 June 2019; Received in revised form 25 July 2019; Accepted 27 July 2019
Available online 31 October 2019

mechanisms activated by the ultrasonic energy, which mainly depend on the specific medium. Another characteristic of high-intensity ultrasonic waves is their capacity to work synergistically with other forms of energy. This is the reason why many practical applications of power ultrasound are not exclusively ultrasonic processes but ultrasonically assisted processes.

The objective of this paper is to present the latest developments of the ultrasonic transducer and power ultrasonic applications. The review contents include the following two aspects: (1) Highlighting the current research trends in magnetostrictive transducer and piezoelectric transducer of different types; (2) Applications of power ultrasound in various industrial fields including chemical reactions, drying/dehydration, welding, extraction, heat transfer enhancement, de-ice, enhanced oil recovery, droplet atomization, cleaning and fine particle removal.

2. Power ultrasonic transducer

Ultrasonic transducer is a device which converts desired electrical signals to ultrasonic waves. Two types of transducers are most widely applied in industrial applications, i.e., magnetostrictive and piezoelectric types.

2.1. Magnetostrictive transducer

A magnetostrictive transducer operates in accordance with the magnetostrictive principle that exhibits interactions between mechanical and magnetic fields in ferromagnetic materials such as iron, nickel, and cobalt. There exists a change in length (size) of a ferromagnetic material if it is subject to an external magnetic field, and the size-changing effect is called the 'Joule effect'. A shearing deformation is formed in a ferromagnetic material when it is subject to a static magnetic field in one direction and a dynamic field from a direction orthogonal to the direction of the static field, and this phenomenon is called the 'Wiedemann effect' [1,2].

The giant magnetostrictive materials are the key technology for developing magnetostrictive transducer. Terfenol-D is a typical magnetostrictive material that can reach strains values between 1000 and 2000 microstrain (i.e. 0.1–0.2%) when subjected to a magnetic field in the 50–200 kA/m range under different temperatures [3]. Due to its high power capacity and fast response speed, the Terfenol-D has demonstrated significant advantages in low-frequency devices and it is necessary to expand the application range of the material to the high frequency field [4,5]. Studies on magnetostrictive-material characterization and constitutive modeling have been made by many researchers. For example, Kim et al. [6] derived a finite element formulation for the coupling of magnetostrictive and elastic materials based upon a separated magnetic and displacement field calculation and a curve fitting technique of material properties. The fluid and structure coupled problem was taken into account based upon pressure and velocity potential fields formulation. Valadkhan et al. [7] evaluated hysteresis models for magnetostrictive materials in terms of accuracy in the presence of minor loops. The model parameters for the Preisach, homogenized energy, and Jiles–Atherton models were identified and validated by experimental data. Jin et al. [8] developed a nonlinear model concerning the multi-field coupling effects. This model considered the effect of temperature on magnetization and could exhibit the strong nonlinear characteristic. Xu et al. [9] proposed a dynamic constitutive model to predict the dynamic hysteresis behavior of giant magnetostrictive materials (GMMs). The model considered the eddy current loss and anomalous loss, and it should be beneficial for the design and control of GMMs actuators. Deng [10] developed a dynamic energy-weighted constitutive model by incorporating stress- and field-induced magnetic field diffusion. The proposed dynamic constitutive model needed much less empirical parameters than the other dynamic magnetostrictive models, only adding the electrical conductivity (a physical property of magnetostrictive materials) to the existing static discrete energy averaged (DEA) model. Shi et al. [11] proposed a quasistatic hysteresis model for magnetoelectric effect in multiferroic nanostructured films based on surface stress model and multi-field coupled hysteretic constitutive model. The model considered the flexural strain for an asymmetric structure consisting of different magnetostrictive phases, and it provided a method to analyze and evaluate the nonlinear magnetoelectric coupling characteristics of self-biased nanodevices operating under extreme stress or temperature conditions.

The ultrasonic transducers based on giant magnetostrictive materials (GMMs) have been focused by people. Stillesjo et al. [12] analyzed the operation of a giant magnetostrictive ultrasonic transducer with a drive current of 10A and frequency of 21 kHz based on a dynamic model. Different power losses have been obtained from a dynamic simulation model of the transducer, which have been used as thermal sources in electro-thermal finite element calculations. It was concluded that the design of a magnetostrictive ultrasonic transducer should comprise an optimal working point regarding magnetic biasing and mechanical pre-stress to minimize the hysteresis. Jammalamadaka et al. [13] fabricated a magnetostrictive transducer operating at 100 kHz using rare earth transition metal giant magnetostrictive material for nondestructive testing (NDT) applications. The 100-kHz giant magnetostrictive transducer was tested through both the ultrasonic through transmission technique and the pitch-catch method for the investigation of defects in a concrete block with delaminated regions. Huang et al. [14] proposed the optimization design method of giant magnetostrictive transducer based on the circuit theory and the system dynamic equations. The finite element method was employed to analyze the resonance frequency of the GMT. The method could be used to optimize the structure of magnetostrictive transducers in order to transfer the maximal energy. Zeng et al. [15] analyzed the magnetomechanical energy conversion and the vibration characteristics of magnetostrictive power ultrasonic transducers. The mathematical model of the Terfenol-D transducer vibrator was developed, and the speed and acceleration expressions of Terfenol-D were deduced by differentiating with respect to displacement equation. Meanwhile, the result of modulation was analyzed from external conditions of transducer and inner structure of magnetostrictive material. Calkins et al. [16] experimentally studied the effect of prestress and bias magnetic field on the dynamic performances (including Young's Modulus, magnetomechanical coupling factor, permeability, dynamic strain coefficient, and mechanical quality factor) of a Terfenol-D transducer. Sheykholeslami et al. [17] designed a resonant ultrasonic transducer with Terfenol-D and investigated the effect of Young modulus of the ferromagnetic material on the dynamics of the transducer including resonance frequency, mode shape, and quality factor. In their other study [18], a GMM transducer working at 8.25 kHz with a high mechanical quality factor and a low damping coefficient was tested based on impedance response analysis in first and second modes. Karafi et al. [19] studied a magnetostrictive resonant torsional vibrator where the longitudinal and circumferential magnetic fields were applied to the patches. The theoretical and experimental results demonstrated that the tip of the horn could generate a high torsional displacement. In their other publication [20], a magnetostrictive torsional resonant transducer (MTRT) was described, and the transducer's structure is shown in Fig. 1. In this transducer a spiral magnetic field was applied to the magnetostrictive horn. The effects of axial and circumferential magnetic fields on torsional displacement of the MTRT were investigated experimentally. The experimental results showed that this transducer resonated at the frequency of 12,325 Hz, while the maximum torsional displacement of the tip of the transducer was 1.2 mrad. These are promising features for industrial applications, such as vibration assisted drilling or plastic welding. An ultrasonic vibration spindle device based on the GMM has been developed, as shown in Fig. 2 [21]. The GMM rod produced a telescopic vibration under the alternating magnetic field generated by the excitation coil, and the vibration was then transmitted to the tool head subsequently to amplification with a horn.

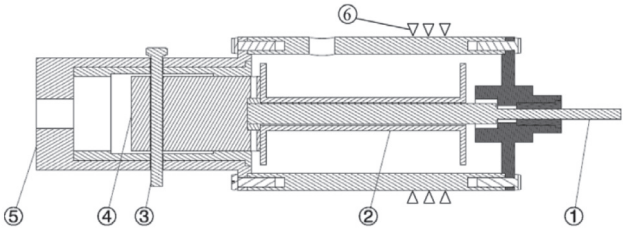

① permendur-horn,②bobbin, ③fixing bolt,
④backing, ⑤aluminum housing, ⑥holding support.

Fig. 1. Structure of the magnetostrictive torsional resonant transducer (MTRT) (Reprinted from [20]).

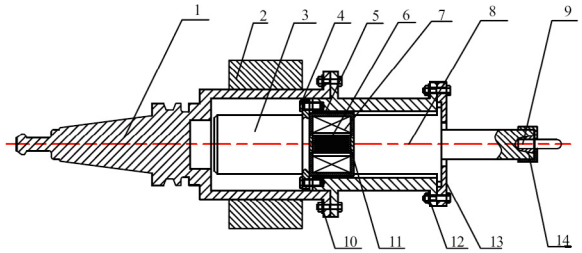

1. tool shank 2. collector ring 3. backing 4. pretension bolt 5. ingot iron 6. GMM
7. magnet exciting coil 8. front shroud (horn) 9. tool head 10. attachment bolt
11. permanent magnet 12. flange bolt 13. flange 14. collet chuck

Fig. 2. Ultrasonic vibration spindle device structure diagram (Reprinted from [21]).

Giant magnetostrictive transducer with Terfenol-D rod exhibits an obvious coupling between deformation and operating conditions such as magnetic excitation, prestress and ambient temperature. To study such coupling effect, a system-level electro-magnetic–mechanical–thermal multifield coupling model of a giant magnetostrictive transducer was proposed in Ref. [22] based on the thermodynamic theory, Jiles–Atherton model, energy balance principle, and structural dynamics principle of the transducer system. In this model, both the temperature-dependent Terfenol-D material properties with dynamic losses and the structural dynamics of the transducer system were taken into account.

The performance of a giant magnetostrictive actuator (GMA) is determined directly by the precision of the GMA output displacement which depends on the coupling deformation displacement due to magnetostrictive deformation and thermal deformation. Experimental study by Wu et al. [23] indicated that the temperature of the GMM rod would exceed 100∘C in the fourth working hour if no cooling measures were taken. So, it was necessary to control the thermal deformation displacement for improving the precision of the GMA output displacement. Usually, the forced cooling measures or constant temperature control methods are used to remove the heat generated by the GMM rod, which ensures the GMM rod temperature accurately remains within a certain small range for achieving a GMA high-precision output displacement. In order to raise the actuating accuracy to nanometric level, Jia [24] designed a water cooling device which used a spiral water cooling tube outside of the GMM rod. Lu et al. [25] proposed a prototype of GMA with double water-cooling vacuums. The study results showed that the cooling system could reduce the thermal displacement to 0.02 μm. Kwak et al. [26] developed a built-in air cooling system to cool the GMM rod. They concluded the optimal running conditions of the cooling systems through a finite element analysis and experimental study. Xu et al. [27] designed a cooling system based on the technology of semiconductor refrigeration for the GMA. To improve the efficiency of semiconductor refrigeration system, the action of water cooling was taken for the heat rejection. The cooling system with semiconductor refrigeration is not economical, and what's more, the cooling capacity cannot be high (normally no more than 100 W). So, the semiconductor refrigeration system is not very suitable for cooling the GMM and GMA. Zhu et al. [28] studied a precise GMA with a heat-induced displacement suppression system which consisted of a temperature control module and a thermal displacement compensation module. The system apparently improved the GMA output displacement precision.

The magnetostrictive transducers which excite and measure guided waves for nondestructive testing (NDT) applications have been developed. Because the magnetostrictive patches are usually flexible and can be fabricated quite easily in any desired form, they are often employed to design magnetostrictive transducers which are called magnetostrictive patch transducers (MPTs). Models and numerical wave simulations related to MPTs were reported. For example, Ref. [29] described an equivalent circuit model of thin-strip magnetostrictive transducers for guided wave generation and detection in structural parts including rods, pipes and plates. The proposed model was effective for estimating the detected waveforms, the frequency response of the transducer and the effect of the thickness of the magnetostrictive strip on the transducer sensitivity. Ribichini et al. [30] established a finite element model which could predict the wave amplitude dependence on significant parameters (including the static bias field, the driving current amplitude and the excitation frequency) of a simple magnetostrictive patch transducer. Oh et al. [31] formulated a finite element procedure and implemented it to predict the wave radiation pattern of a magnetostrictive patch transducer installed on a plate. The procedure was featured by a linearized model which determines coupling matrix appearing in the magnetostrictive constitutive equation of a magnetostrictive patch in a transducer.

For the MPTs that were developed for pipes/rods inspection, they normally worked in longitudinal [32] or torsional [33–37] wave modes. Among various guided waves, the guided torsional wave played a unique role in cylindrical waveguides because its fundamental mode was nondispersive. For this reason, Cho et al. [33] developed a specially configured meander coil-magnetostrictive patch transducer (see Fig. 3) which could detect a small-sized crack with guided pure torsional waves of up to 2 MHz. In this MPT, flexible magnetostrictive patch which had strong magnetostriction was used and tightly bonded onto a test cylindrical waveguide using epoxy resin to overcome the difficulty of induction of torsional waves with sufficient power as the magnetic field was directly applied to a typical cylindrical waveguide. A meander coil was designed to cover most part of the magnetostrictive patch, which supplied a dynamic magnetic field to the patch. In addition, two permanent magnets with the specified polarities were proposed to stably provide bias magnetic field which is important in the generation of torsional waves, especially for the high-frequency range. The pipe-specific MPTs that used the Wiedemann and its reverse effects for the transduction of torsional waves can be found as well in Ref. [34–36]. Various applications of pipe-specific MPTs include inspections of various defects of rotating shafts [37] and pipes [38–40].

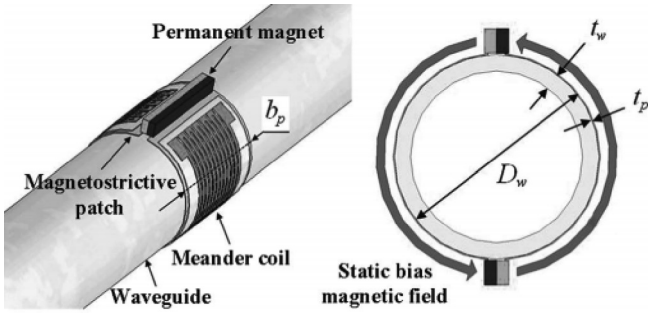

Fig. 3. Schematic diagram of the proposed magnetostrictive patch transducer by Cho et al. [33].

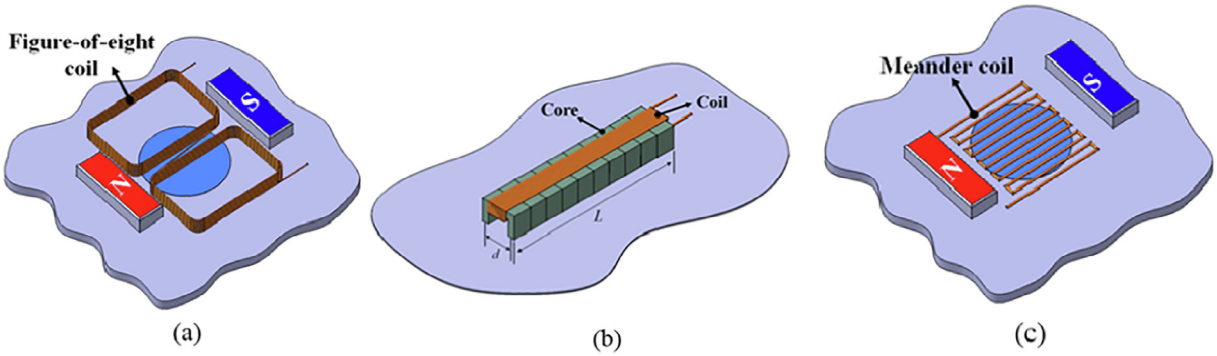

Fig. 4. Various Magnetostrictive patch transducer (MPT) using (a) a figure-of-eight coil, (b) a coil wound around a core and (c) a meander coil (Reprinted from [44]).

Another type of MPTs that were developed for plate applications [41] can generate directional [42–46] or omni-directional Lamb and shear-horizontal (SH) waves [47–49]. Fig. 4 shows some examples of plate-type MPTs [44]. The first MPT (Fig. 4(a)) is used for generating SH waves [43], the second (Fig. 4(b)) can generate high-power SH waves because a coil is wound around a core [50], and the third configuration using a meander coil aims at improving the directivity or frequency tuning characteristics [51]. The plate- specific MPTs were not only used for imaging [52], but also for intriguing experiments involving phononic crystal [53,54] and metamaterial plates [55]. The other applications of the plate-specific MPTs can be found in the elasticity modulus measurement [56] and structural health monitoring [57,58].

Known from the above literature, the magnetostrictive transducers are capable of providing vibrations over a wide frequency range (e.g., 17–23 kHz for a 20 kHz generator) which provides higher flexibility in the design of horn and wear adjustments. Meanwhile, the magnetostrictive transducers can generate and measure ultrasonic waves at frequencies ranging between roughly 20 kHz and 1–2 MHz for non-destructive testing (NDT) of waveguides such as pipes and plates. However, major issue with the magnetostrictive transducer is the electrical energy dissipation in the form of heat which needs extra cost and weight of cooling system.

2.2. Piezoelectric transducer

A piezoelectric transducer consists of one or more disks of piezoelectric material sandwiched between two metal sections. The entire assembly is resonant at a predetermined frequency, and its length is acoustically equal to one-half wavelength at the applied frequency. Compared with the magnetostrictive ultrasonic transducer, the piezoelectric one has merits such as simple structure, no electromagnetic radiation, high energy density, low cost and so on. Hence, the piezoelectric method for generating ultrasonic waves has been increasingly focused by people. There are many kinds of piezoelectric transducers that can be excited to vibrate in different vibrational modes for different practical applications. Generally speaking, there are four fundamental vibration modes, i.e. longitudinal mode, radial mode, flexural (or bending) mode and torsional mode. Any two of these modes can constitute a complex vibration mode, e.g., the longitudinal-flexural, the torsional-flexural and the longitudinal-torsional.

2.2.1. Longitudinal transducer

An ultrasonic longitudinal transducer is generally a solid rod with different shape function of ultrasonic horn whose profile can be stepped, conical, exponential, and etc. Many designs have been concentrated on the solid horn structure to amplify the vibration displacement of the longitudinal transducers. For example, Wang et al. [59] designed a Bezier-spline profiled horn with high displacement amplification for ultrasonic welding. Prototype of the new ultrasonic horn has been manufactured by a numerical control machining process, and the experimental study manifested that the displacement amplification of the proposed horn was 71% higher than that of the traditional catenoidal one with the same length and end surface diameters. After that, they further developed another new ultrasonic horn with the profile of B-spline curve [60]. The B-spline profiled horn has been proved to have the higher displacement amplification than the traditional catenoidal horn and the Bezier profiled one with the same length and end surface diameters. Rani et al. [61] studied the different horn profiles used for ultrasonic welding of thermoplastics by using modal and harmonic analysis. Xu et al. [62] established a theoretical model for the cup-shaped ultrasonic transducer which had significant applications in ultrasonic machining, such as continuous bonding of plastic sheet or strips and investigates the vibrational characteristics of the cup-shaped ultrasonic transducer by using the analytical and numerical methods. Zhang et al. [63] derived an electromechanical coupling model for the longitudinal vibration type piezoelectric ultrasonic transducer with an exponential horn which could efficiently focus energy to enlarge vibration amplitude and velocity. The analytical model could be used for the langevin type longitudinal transducer design and optimization. Grabalosa et al. [64] studied the stepped sonotrode in ultrasonic molding technology by using the finite element method and obtained a frequency map providing the dimensional range within which the sonotrode could be re-machined in order to eliminate tool wear. In all these studies, different horn shapes or structures were selected and designed according to the conventional design theory to satisfy specific objective, and different horns with different shapes and dimensions were required for different ultrasonic applications. To solve this problem, longitudinal step-type ultrasonic horns with adjustable performance were proposed by Lin et al. [65]. In this kind of ultrasonic horn, piezoelectric material was inserted in the horn and connected with external electric impedance, and the horn performance could be adjusted by changing the electric impedance and the location of the piezoelectric material in the horn.

The V-shaped sandwich piezoelectric transducer initially proposed by Kurosawa et al. in 1998 [66] is the most typical longitudinal-longitudinal coupling vibration transducer used to drive sliders to construct a linear ultrasonic motor. The V-shaped piezoelectric transducer normally consists of two Langevin piezoelectric transducers connecting together at a joint tip with a fixed angle, and the two longitudinal vibration modes are, respectively, stimulated in these two Langevin transducers and then coupled in the joint tip, resulting in an elliptical motion of the joint tip. The V-shaped piezoelectric transducers can oscillate with relatively high amplitude and be employed for both linear and rotary displacements [67–69]. Suzuki et al. [70] developed a V-shaped transducer with an acute angle between two Langevin transducers which were used to generate the vertical and horizontal vibration components. The complex vibration was excited by using two electrical sources with a phase shift. Since the ultrasonic vibrations have unique characteristics such as silent motion and absence of magnetic noise, the motor based on the V-shaped transducer are suitable for

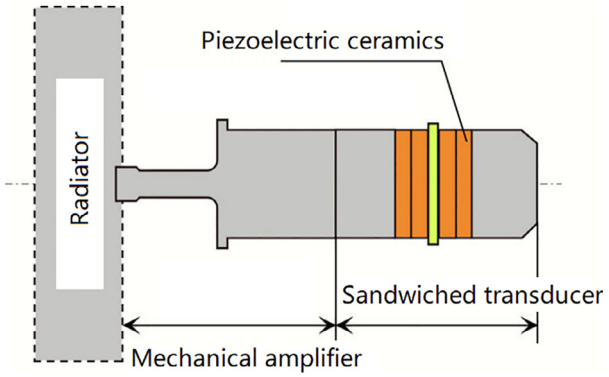

Fig. 5. Basic structure of the transducers [74].

medical bed applications in hospitals. Because of its favorable output performance, the V-shaped transducer has been further employed as machining tools for elliptical vibration surface texturing manufacturing [71]. To study the influence of the coupling angle and cross-section on modal characteristics and electromechanical coupling coefficient, Li et al. [72] has built an electromechanical coupling model of a V-shape piezoelectric ultrasonic transducer considering the longitudinal and lateral movements of a single beam. Recently, Wang et al. [73] developed a simple semi-analytical model for the proposed three-dimensional transducer by utilizing the transfer matrix method (TMM) which was considered as a precise tool and offered efficient solution to describe the dynamic behaviors of complex systems including any traditional V-shaped transducers.

A new family of high power ultrasonic transducers with extensive radiators for specific uses in fluids (especially gases) and multi-phase media have been recently introduced. J.A. Gallego-Juárez et al. [74] proposed and investigated a radiator structure with properly designed slots for acquiring high acoustic power capacity, high efficiency and controlled radiation patterns. The basic structure of such transducers is schematically shown in Fig. 5. It consisted essentially of a piezoelectrically activated vibrator which drives an extensive radiator. The vibrator, which was generally a circular or rectangular vibrating plate with stepped, grooved or stepped-grooved profile, consisted of a sandwiched piezoelectric ultrasonic transducer and a solid horn which acts as a vibration amplifier. The extensive surface area of the radiator increased the radiation resistance and helped the vibrating system have good impedance matching with the medium. The vibration distribution and the radiation pattern could be controlled through the particular design of the radiator adapted to specific situations. Meanwhile, the fundamental frequency and displacement distribution of the stepped plate can be controlled as well by the operation frequency of the longitudinal transducer at its center [75]. Xie et al. [76] established the dependence of arc acoustic binding on three concave radiator surfaces, i.e., paraboloid of revolution, spherical cap surface and rotating single curved surface. The study results manifested that a redesign of the radiator configuration could provide an alternative solution that possibly enhanced both acoustic pressure level and arc-acoustic interaction. To generate a more evenly distributed acoustic field, Wang et al. [77] designed an ultrasonic horn with stepped-plate radiator configuration as shown in Fig. 6. The ultrasonic vibration system was based on the longitudinal vibration of a variable cross-section horn, which was used for gas tungsten arc welding in which the ultrasonic wave was emitted from the stepped-plate radiator and reflected by the reflector (workpiece surface).

A new topological structure for the Langevin-type transducer has been proposed and investigated by Lu et al. [78]. As depicted in Fig. 7, the two cylindrical terminal blocks were conically shaped with four support plates each, and two cooling fins were disposed at the bottom of the terminal blocks and adjacent to the piezoelectric rings. Due to the

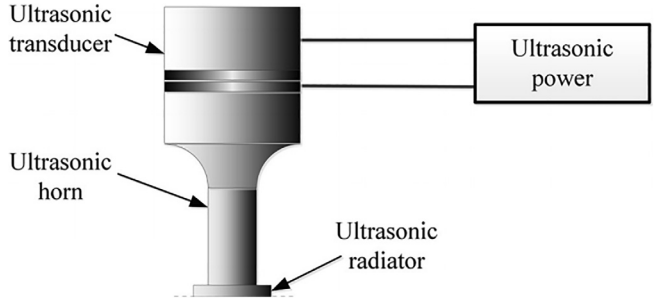

Fig. 6. Schematic diagram of the ultrasonic transducer for gas tungsten arc welding (GTAW) [77].

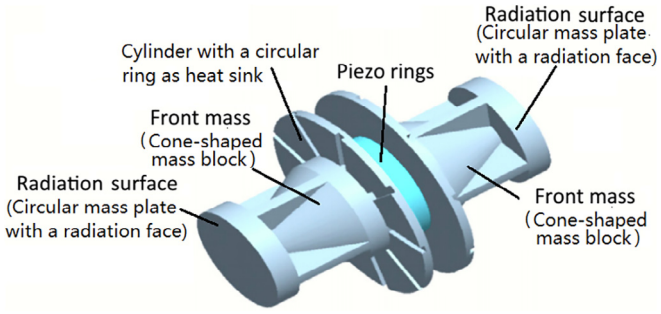

Fig. 7. Basic structure of the transducers [78].

decrease of mass and force factor and the increase of the heat dissipation surface, the proposed transducer had the larger vibration amplitude, acoustic output power and electroacoustic energy efficiency, and lower temperature rise than the traditional Langevin transducers at the same driving voltage and resonance.

2.2.2. Radial transducer

Piezoelectric ring transducers are a kind of well-developed high power acoustic transmitters. There are a number of previous studies on the vibrational characteristics of the axisymmetric vibration of axially polarized piezoelectric rings. Kim et al. [79] derived dynamic differential equations of piezoelectric radial motion in terms of radial displacement and electric potential considering the piezoelectric anisotropy and studied the radial vibration characteristics of piezoelectric cylindrical transducers with radial polarization. Lin [80] established electro-mechanical equivalent circuit model for the piezoelectric ceramic thin circular ring in radial vibration based on which the relationship between the resonance frequencies and the material parameters and the geometrical dimensions was analyzed. To increase the power capacity of the cymbal transducer, a radial composite piezoelectric transducer, which was composed of a piezoelectric ceramic ring sandwiched between two metal rings in the radial direction as shown in Fig. 8, was put forward and studied by Lin [81] by using the electro-

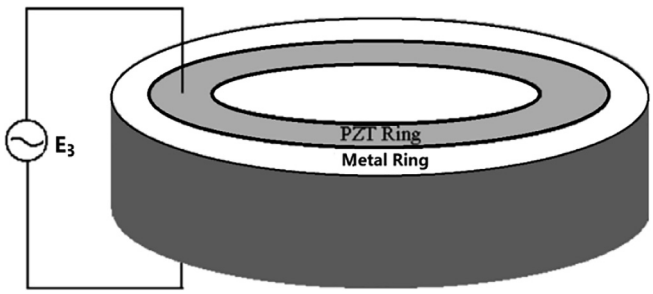

Fig. 8. Schematic diagram of a radial composite piezoelectric transducer in radial vibration [81].

mechanical equivalent circuit model.

Afterwards, Lin et al. [82] established the three-port electro-mechanical equivalent circuit of the piezoelectric ceramic tube in radial vibration which could be used to investigate the radial vibration of the radially poled piezoelectric ceramic long tubes with arbitrary wall thickness. Wang et al. [83] derived the resonant frequency of piezoceramic ring according to the piezoelectric constitutive and kinematical equation which could be employed to study the vibration property of the radially polarized piezoelectric rings. Ye et al. [84] developed a unified model for the free vibration analysis of thick cylindrical shells with general end conditions and resting on elastic foundations based on the three-dimensional theory of elasticity. In this model, each shell displacements was expanded as a standard Fourier cosine series with four auxiliary functions which were introduced to eliminate any possible discontinuities of the original displacement. The model could be universally applied to a variety of end conditions including all the classical cases and their combinations as well as arbitrary elastic foundations and may serve as benchmark solutions for validating new computational techniques in future. In the study by Wang et al. [85], the model for the radial vibration behavior of functionally graded piezoelectric ring transducers resting on elastic foundation has been established, and based on the proposed model, the design parameters (including resonant/anti-resonant frequencies, effective electromechanical coupling factor and model shape) were analyzed. The study indicated that the resonant and anti-resonant frequencies could be increased or decreased by adjusting the elastic foundation stiffness or material inhomogeneity index.

2.2.3. Flexural/bending transducer

As another important vibration mode of the ultrasonic transducer, the flexural/bending vibration characteristics could be utilized for biomedical applications. For example, Sunny et al. [86] designed a flexural transducer (20–100 kHz) that could deliver maximum displacement amplitude with the lowest possible excitation voltage and be capable of tether-free, self-contained battery operation for clinical applications. Further, they optimized individual flexural piezoelectric elements by using a finite-element model [87].

A Langevin type transducer which is composed of an exponential horn, four groups of PZT ceramics and a back beam was constructed by Zhang et al. [88]. The exponential horn could focus the vibration energy and enlarge vibration amplitude and velocity efficiently. To guide the design of such kind of transducer, an electromechanical coupling model was established based on the vibration model, which could be used to determine the most reasonable excitation position of PZT ceramics.

In Ref. [89], a unimorph flexural transducer design was proposed and tested in terms of mode shapes and frequencies. The unimorph flexural transducers consisted of a passive metal cap structure and a thin piezoelectric disc tightly bonded to the inside. Meanwhile, a finite element model has been established and experimental 2D, time-resolved displacement measurements were performed to analyze the transducers flexural properties.

To realize on-chip manipulation of microparticles in small channels through ultrasonic vibration, Yamamoto et al. [90] attached four lead zirconate titanate transducers to four corners of a chip which consists of a rectangular glass substrate with a cross-shaped channel. And in order to efficiently generate the flexural vibration mode on the chip, they also used finite element analysis to optimize the configurations of the glass substrate and transducers. Through controlling the driving phase difference between the two pairs of transducers, the acoustic standing waves moved in the same direction, and the particles could be manipulated by the two-phase drive.

The transducers with flexural vibration mode have the higher requirements those with longitudinal vibration modes in terms of the manufacture and assembly of the flexural vibration piezoelectric ceramics because the flexural vibration produces a shear force on the piezoelectric ceramics that can easily result in the breakage of ceramics. To overcome the complex polarizations and configurations of flexural vibration piezoelectric ceramics, a novel sandwiched type flexural piezoelectric transducer utilizing common rectangular longitudinal vibration piezoelectric ceramics was proposed by Wang et al. [91]. The proposed transducer has a simple and compact structure and it is easy to excite the flexural vibration by varying the temporal phase differences of the excitation signals.

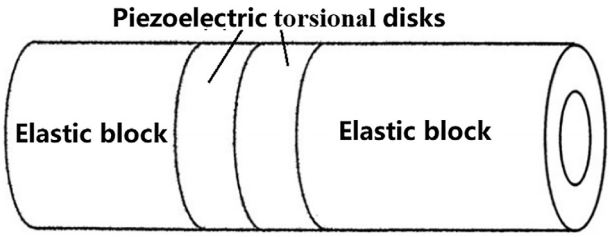

Fig. 9. Schematic for torsional transducer [92].

2.2.4. Torsional transducer

Torsional transducers are more complicated than the longitudinal and radial transducers. The torsional transducers are normally made by: 1) assembling polarized cubes; 2) polarizing the even number of sectors of a disk and covering it with alternate electrodes; and 3) circumferentially polarizing a disk. Fig. 9 shows typical shape of the torsional transducer in which the torsional disks are usually of high-frequency resonance and are assembled with two elastic blocks at both ends by using a bolt to lower the resonance frequency [92]. The piezoelectric torsional disks for the torsional transducer could be fabricated through the following critical processes [92]: 1) A disk molded with ceramic powder was divided into an even number of sectors, and the alternate sectors were painted with silver electrodes; 2) Polarizations of the sectors were made in the circumferential direction by using a couple of adjacent electrodes driven by electric voltage; 3) The divided electrodes were removed after polarization; 4) Other electrodes were painted on the top and bottom surfaces of the disk, and the electrodes were connected to a driving circuit.

The ultrasonic torsional transducer can be employed to generate micro droplets. Harada et al. [93] designed a torsional bolt-clamped Langevin-type transducer for liquid atomization. As shown in Fig. 10 [93], the transducer was constructed by stainless steel blocks, a stainless steel bolt, and piezoelectric elements whose polarization was in the circumferential direction to generate a torsional vibration. The micropore that was placed at the same distance from the center was equally oscillated by using the torsional vibration mode. Kiyama et al. [94] further studied the vibration mode of the ultrasonic torsional transducer by using a finite element method. Meanwhile, the relationship between frequency, admittance, and phase as well as the relationship between frequency and circumferential vibration amplitude were investigated.

The torsional vibration mode can be employed for tissue characterization applications in the field of clinical diagnosis because the

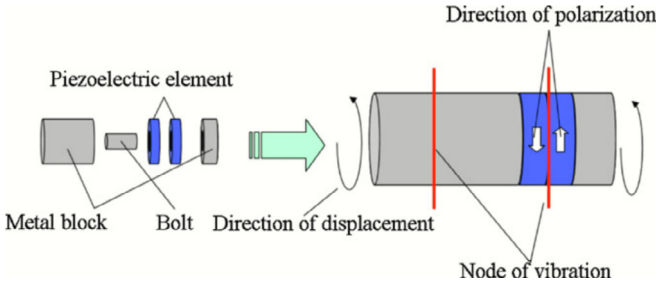

Fig. 10. Schematic for the torsional transducer studied in Ref. [93].

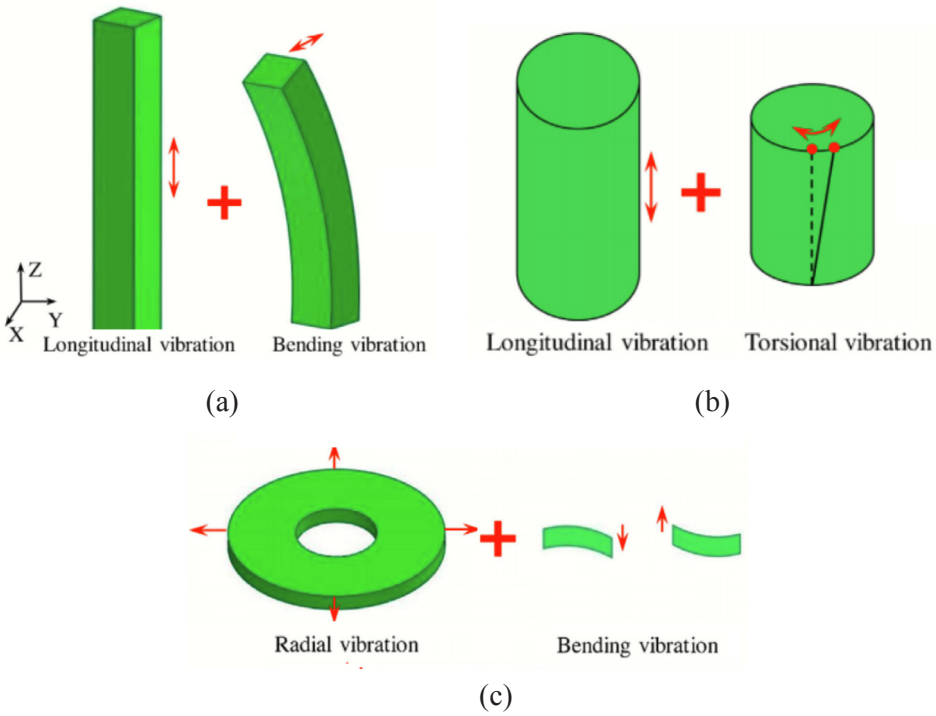

Fig. 11. Composite vibration mode (a) Longitudinal-flexural (or bending); (b) Longitudinal-torsional; (c) Radial-flexural (or bending) [97].

torsional waves propagate at the S-wave speed have been reported to be significantly sensitive to consistence changes in quasifluids and soft tissues [95]. Melchor et al. [96] proposed a torsional piezoelectric ultrasonic sensor for detecting shear stiffness properties of soft tissue which were correlated with a number of pathologies like tumors, hepatic lesions and so on. The torsional transducer was composed by a combination of elastic and piezoelectric parts, and the PZT-5 was adopted for the transducer design.

2.2.5. Composite vibration transducer

The sandwiched type piezoelectric transducers can be designed to operate in composite vibration modes for some specific applications. These mainly include composite longitudinal-flexural (or bending) vibration, composite longitudinal-torsional vibration and composite radial-bending vibration, as shown in Fig. 11 [97]. As indicated from Table 1, the combinations of the longitudinal vibration mode with the other vibration modes (i.e., the bending or the torsional) are the major research topics.

The composite vibration transducers are often employed to fabricate new-type motor (called ultrasonic motor). Fig. 12 shows an ultrasonic motor with a longitudinal PZT and a bending PZT [98]. The stator was composed of one cylinder and one longitudinal and bending composite transducer located on the outer surface of the cylinder in radial direction, and the transducer included an exponential shape horn located on the leading end. Typical output of the prototype motor had no-load speed of 281 rpm and maximum torque of 1.2Nm at an exciting voltage of 200 V rms.

Fig. 13 gives a new linear ultrasonic motor designed by Yang et al. [99]. In this new design, two exponential shape horns were located on the two ends to magnify vibration amplitude and velocity. Two groups of bending PZT ceramics were sandwiched between flange bolt and horns, and Beryllium bronze sheets were clamped to serve as electrodes. The friction material blocks which were bonded on the end tips of the horns served as the driving feet. The proposed motor could generate elliptical motion at the driving feet by superimposing longitudinal and bending vibrations with phase difference temporally.

Wang et al. [104] proposed a resonant type piezoelectric stepping motor (See Fig. 14) which included eight longitudinal PZT plates for exciting the first longitudinal vibration and eight bending PZT plates for exciting the second bending vibration of the motor. According to the test, the prototype motor could acquire a velocity of 13.45 mm/s at the input voltage of 320 $V_{p\text{-}p}$ and the frequency of 100 Hz, and the maximum thrust force was identified as about 18 N under voltage and preload of 200 $V_{p\text{-}p}$ and 100 N. The proposed stepping motor was featured by compact structure, high output velocity and large thrust force.

Chen et al.[112] fabricated a new ultrasonic motor by using the radial bending mode of a thick ring. Fig. 15 shows the basic structure of the proposed motor. In the new design, PZT stacks and block springs were nested alternately into the slots to ensure that uniform preloading was applied to the PZT ceramics. The prototype motor could achieve a maximum torque of 1.0 N·m and a maximum power of 5.2 W. The ultrasonic motor was featured by the utilization of the radial bending mode which allows all driving points to have an identical pushing effect on the rotor and the reduction of static capacitances of the PZT elements which brought about the higher electromechanical coupling factor and the less energy loss in the interfaces.

The composite vibration ultrasonic transducers were also used for developing high-performance actuators which usually push the runners by the resonant movements on the surface particles. Fig. 16 presents a novel standing wave linear piezoelectric actuator [100]. In such actuator, a new longitudinal-bending coupling mode was generated in a sandwich transducer to produce oblique elliptical movement on the driving tip. According to the experimental study, the standing wave linear piezoelectric actuator could achieve maximum no-load speed of about 891.3 mm/s and thrust force of about 39.2 N when the input voltage was 400 $V_{P\text{-}P}$ and the working frequency was 29.4 kHz.

Fig. 17 gives a stepping piezoelectric actuator designed by Shen et al. [103]. This piezoelectric actuator consisted of a base, a linear guider and two longitudinal-bending hybrid transducers, and a linear guider was fixed on one side of the base as a runner. The experimental study manifested that the proposed stepping piezoelectric actuator could achieve a long travel motion with resolution of 50 nm, and the maximum stepping displacement and the maximum speed were tested to be 10.75 μm under the voltage of 400 $V_{p\text{-}p}$ and 720.65 μm/s under

Table 1
Typical studies on the composite vibration transducers since from 2010.

Composite vibration mode	Ref. [No.] /Year	Highlights
Longitudinal-flexural (or bending)	Ref.[98]/2010	A cylindrical type traveling wave ultrasonic motor was fabricated by using longitudinal and bening composite transducer. The output of the prototype motor was no-load speed of 281 rpm and maximum torque of 1.2 N.m at an exciting voltage of 200 V_{rms}.
	Ref.[99]/2013	The longitudinal and bending vibrations of ultrasonic transducer were employed for fabricating a new linear ultrasonic motor. The prototype motor achieved a maximum speed of 560 mm/s and a maximum output force of 55 N at a voltage of 450 V_{p-p}.
	Ref.[100]/ 2016	A novel standing wave linear piezoelectric actuator was proposed by using a longitudinal-bending sandwich transducer. The proposed standing wave linear piezoelectric actuator achieved maximum no-load speed and thrust force of about 891.3 mm/s and 39.2 N under voltage of 400VP-P and working frequency of 29.4 kHz.
	Ref.[101]/ 2017	A novel ultrasonic drill method with longitudinal-bending hybrid ultrasonic vibration was reported. The longitudinal vibration was employed to cut the edge, and the bending vibration speeds up the movement of the cutting edge.
	Ref.[102]/ 2017	A new transfer matrix model was established for the composite piezoelectric beam to describe the coupled longitudinal and bending vibrations.
	Ref.[103]/ 2018	A linear stepping piezoelectric actuator was fabricated by using two longitudinal-bending hybrid transducers. The maximum stepping displacement was tested to be 10.75 μm under voltage of 400 V_{p-p}, the maximum speed is 720.65 μm/s under frequency of 60 Hz and the maximum thrust is about 15 N.
	Ref.[104]/ 2019	A resonant type stepping motor using a bolt-clamped transducer was proposed. The two exciting signals applied to the longitudinal PZT plates and bending PZT plates have a phase shift of /2.
	Ref.[105]/ 2019	A longitudinal-bending coupling vibration transfer matrix was established for improving the performance of the combined PZT elements.
Longitudinal-torsional	Ref.[106]/ 2012	The working efficiency of longitudinal–torsional vibrations of two types of ultrasonic step horns were studied by using both numerical and experimental methods.
	Ref.[107]/ 2013	The numerical, analytical and experimental methods were used to estimate the longitudinal-torsional (L-T) transducer electro-mechanical parameters for different geometric modifications.
	Ref.[108]/ 2015	A new sandwich longitudinal–torsional (L&T) composite ultrasonic vibrator was proposed for wire drawing.
	Ref.[109]/ 2017	A sandwich longitudinal-torsional (L & T) composite ultrasonic vibrator driven by a longitudinally polarized PZT stack was presented.
	Ref.[110]/ 2019	A novel longitudinal & longitudinal-torsional (L-LT) actuator was fabricated, and the prototype achieved a maximum speed and torque of 193r/min and 0.065 N.m, respectively.
Radial-bending	Ref.[111]/ 2012	A rotary traveling wave ultrasonic motor (USM) was constructed by using radial bending mode of ring with nested PZT excitation. The maximal speed and torque of the prototype are tested to be 126 r/min and 0.8 N center dot m, respectively.
	Ref.[112]/ 2014	A traveling wave ultrasonic motor utilizing a radial bending mode of a thick ring is proposed. The prototype achieves maximum speed and torque of 146 r/min and 1.0 N·m, respectively.

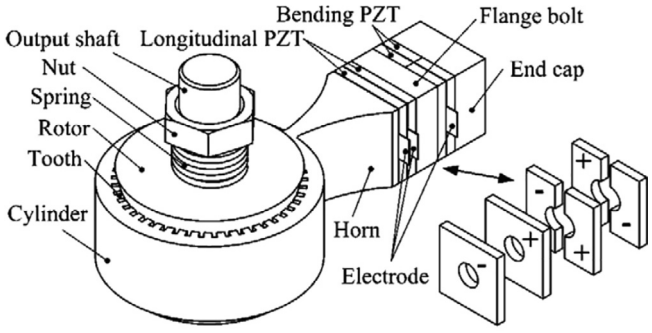

Fig. 12. Schematic diagram of the ultrasonic motor proposed by Liu et al. [98].

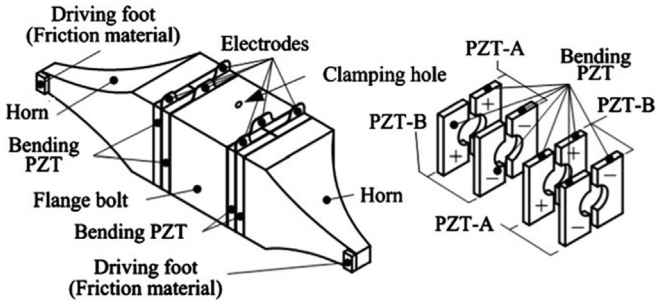

Fig. 13. Schematic diagram of a new linear ultrasonic motor proposed by Yang et al. [99].

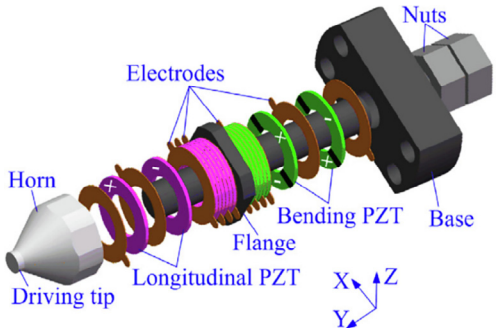

Fig. 14. Schematic diagram of the piezoelectric stepping motor [104].

the working frequency of 60 Hz, respectively.

3. Applications of power ultrasound

The application of high-intensity ultrasonic waves is based on the potential effects of power ultrasound mainly including mechanical and thermal effects in a medium and cavitation in liquids. These special effects of power ultrasound can be employed to produce or to enhance a wide range of processes that largely depend on the specific irradiated medium, i.e., solid medium, liquid medium and gas medium, as shown in Fig. 18.

There has been a renewed interest in the industrial applications of power ultrasound including dehydrating, welding, de-icing and wire bonding in solids, and chemical reactions, atomization, cleaning, extraction, oil recovery and heat transfer enhancement in liquids, as well as drying, fine particle removal and defoaming in gas.

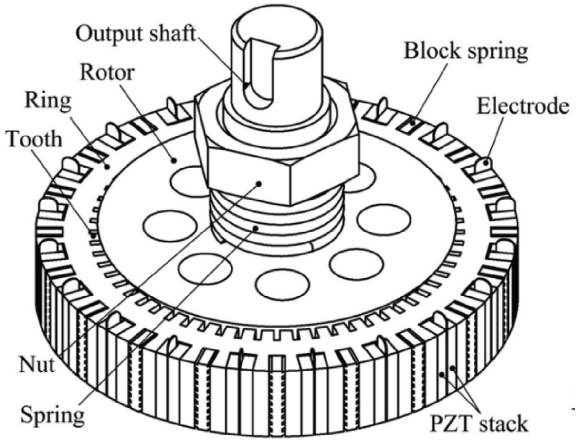

Fig. 15. The three-dimensional model of a traveling wave ultrasonic motor utilizing a radial bending mode of a thick ring [112].

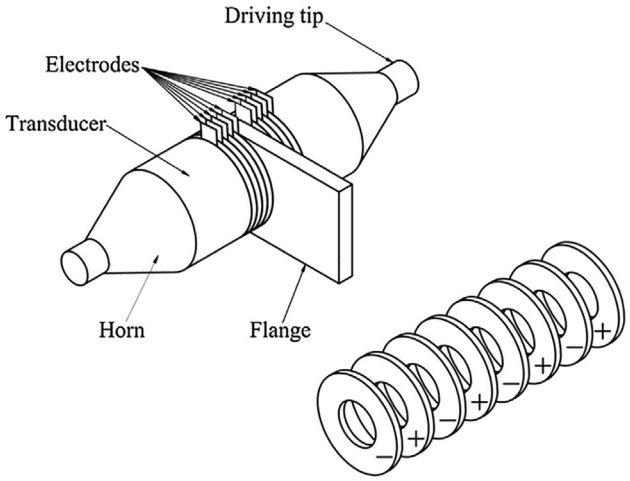

Fig. 16. Structure of the standing wave linear piezoelectric actuator proposed by Liu et al. [100].

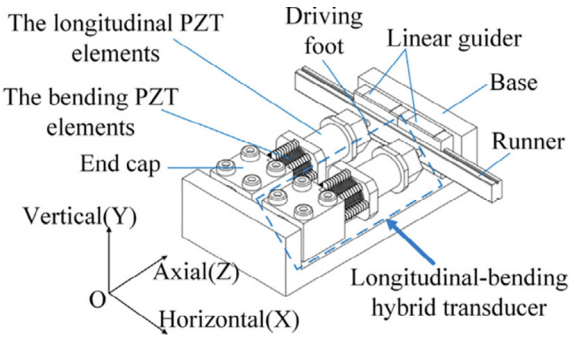

Fig. 17. Structure of the stepping piezoelectric actuator proposed by Shen et al. [103].

3.1. For chemical reactions

The effect of power ultrasound on the chemical processes is mainly due to the acoustic cavitation in the case of liquid environment. The formation, growth and implosive collapse of cavities in liquids that release highly localized energy with very high temperatures and very high pressures in few microseconds brings about chemical or physical changes and promotes transport processes within the reaction medium. In addition, the high temperature and high-pressure region of acoustic cavitation bubbles generate strong oxidizing substances like H_2O_2 and ·OH radicals that may participate in a chemical reaction [113] or degrade non-volatile polar organic compounds in water [114].

In the last decade, power ultrasound has been extensively applied to different types of chemical reactions aiming at intensifying the reaction processes with higher yield of product in short time. These chemical reactions are Mannich-type reactions, Aza-Michael reactions, stille coupling reactions, oxidation reactions, phase transfer catalyzed reactions and chemical synthesis as well as catalytic transesterification process, as summarized in Table 2 [115–126]. According to the studies, the potential benefits of power ultrasound brought for the chemical reactions include much higher reaction rate or shorter reaction time, lower energy consumption, better catalyst effectiveness and less use of hazardous raw materials participating in the chemical processes.

To promote the applications of power ultrasound in chemical reactions, sonochemical reactors have been designed and studied in terms of controlling mechanism, reaction kinetics and optimal operation parameters. Basically, there are two types of ultrasonic irradiation modes for the sonochemical reactors. One is direct irradiation mode in which the ultrasonic transducer is in direct contact with reaction medium, and the other is indirect mode in which the ultrasonic transducers are attached to the wall or the bottom of the vessel and not in direct contact with reactants. There have developed some modifications of the sonochemical reactors. For example, the ultrasonic airlift loop reactor has been proved to be an advisable choice for chemical reactions [127]. Asakura et al. [128] developed a large sonochemical reactor by using 12 PZT transducers with the working frequency of 500 kHz and total effective electric power of 620 W. Meanwhile, the operating parameters such as ultrasonic power, frequency, duty cycle and temperature were always considered by people for the better use of power ultrasound in chemical reactions. It is easily understood that the higher ultrasonic power results in the higher cavitational intensity which makes the reactions become faster. There should be an optimum power beyond which a further increase in the power produces small effect on the chemical process [129]. It is also important to understand that with the frequency of power ultrasound increasing, the chemical effects induced by the power ultrasound will increase and the physical effects like circulation and turbulence will decrease. Study by Francony et al. [130] indicated that the higher frequency of power ultrasound up to 500 kHz would produce the higher quantum of free radicals as compared to the lower frequency of power ultrasound. Therefore, there ought to be an optimum frequency under which the maximum process intensification benefits can be obtained by power ultrasound.

Overall, the power ultrasound offers considerable potential for green and sustainable chemical processing. Efficient scale up procedures and corresponding equipments are required to be developed for industrial applications.

3.2. For drying/dehydration

The development of modern and high-power ultrasonic transducers in recent years promotes the applications of ultrasonic drying. It has been found that ultrasounds could work synergistically with other drying techniques, such as convective drying [131–137], microwaves [138–140], vacuum [141–147] and freezing [148–153], to accelerate the drying process. The recent studies on the hybrid drying method with ultrasound are listed in Table 3. From these studies, it can be seen that the introduction of ultrasound to the drying could greatly accelerate the drying process and shorten the drying time without causing a noticeable temperature increase in the materials. Therefore, the ultrasound-assisted drying method is very suitable for temperature-sensitive food like apples, peas, strawberry, grapes, and so on.

The application airborne ultrasound in convective drying is mainly linked to its mechanical effects. On one hand, high frequency vibration induced by ultrasound causes a micro vibrations and air turbulences near the material surface, which enhances the heat and mass transfer process. On the other hand, the transmission of ultrasonic waves

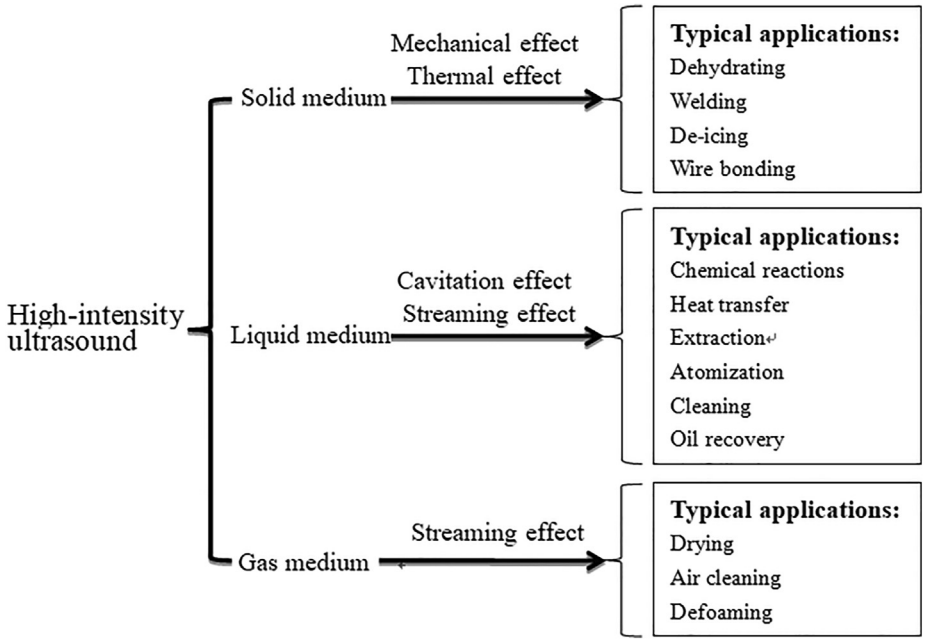

Fig. 18. Applications of power ultrasound in different mediums.

Table 2
Applications of power ultrasound in chemical processes.

Type of reactions	US conditions	Main results	Ref.[No.]/ Year
Mannich-type reactions	UP: 600 W UF: 40 kHz	It took 18 h for high speed stirring to have 88% of product yield, while ultrasound assisted process could obtain 95% of product yield in only 1.5 h	Ref. [115]/ 2009
Aza-Michael reactions	UP: 135 W UF: 42 kHz	Remarkable enhancement of reaction rate has been observed in water under ultrasound-induced method. By using conventional stirring, it needed 30 min for achieving 92% reaction yield, whereas the application of power ultrasound reduced the reaction time to 5 min and improved yield of 98%.	Ref. [116]/ 2012
Stille coupling reactions	UP: 600 W UF: 20 kHz	A significant intensification was reported due to the use of ultrasound with the required reactiontime decreasing from 20 h (for the conventional approach) to 30 min. Meanwhile, ultrasound significantly enhanced the rate of reaction resulting in 97% yields which is much higher than the conventional method.	Ref. [117]/ 2012
Oxidation reactions	UI: 1.26 W/mL UF: 20 kHz	According to this study, conventional heating at 90℃ gave yield of 97% in 60 min., whereas ultrasound assisted process achieved 98% of product yield in only 15 min.	Ref. [118]/ 2014
Lutein disuccinate synthesis	UP: 300 W UF: 45, 80 and 100 kHz	Ultrasound improved the limiting equilibrium conversion from about 56% in 12 h of conventional method to about 80% in only 2 h.	Ref. [119]/ 2014
Multi component synthesis	UP: 80 W UF: 35 kHz	Ultrasound assisted synthesis could obtain 95% product yield in 10 min which was much more efficient as compared to the conventional approach for the synthesis of twelve novel derivatives.	Ref. [120]/ 2015
Synthesis of glycerol carbonate catalyzed by lipase	UP: 0–200 W UF: 25 and 40 kHz	Ultrasound could obtain limiting equilibrium conversion of 99.75% and need 10 h less time than the stirring method.	Ref. [121]/ 2015
Phase transfer catalyzed reactions	UP: 200 W UF: 40 kHz	Ihe ultrasound assisted phase transfer catalyst (US-PTC) based approach was more efficient than conventional approach in the conversion of 4-chloronitrobenzene.	Ref. [122]/ 2018
Homogeneous acid-catalyzed transesterification	UP: 130 W UF: 40 kHz	The new single-step ultrasound production of biodiesel from high fatty acid D.metel Linn oil using sulfuryl chloride as catalysts could achieve 95.50% yield in 2 h.	Ref. [123]/ 2016
Heterogeneous base-catalyzed transesterification	UP: 210 W UF: No reported	The SrO-CaO catalyst exhibited high efficiency towards converting Jatropha oil into biodiesel by ultrasonic-assisted transesterification.	Ref. [124]/ 2016
Interesterification	UP: 80 W UF: No reported	Ultrasound assisted interesterification was a fast and efficient approach for biodiesel production giving significant benefits including significant reduction in the reaction time with higher yields and lower requirement of the enzyme loading.	Ref. [125]/ 2016
Heterogeneous acid-catalyzed transesterification	UP: 100 W UF: 37 kHz	Esterification of oleic acid by various alcohols was achieved with high yields under ultrasonic irradiation	Ref. [126]/ 2017

through the body causes a rapid series of contractions and expansions of the material tissue (also called 'sponge effect') and creates microscopic channels which make moisture dehydration easier. Acoustic energy also contributes to a moderate temperature rise in material and causes an increase in water vapor pressure in the dried body. There have developed some ultrasound-assisted convective drying systems. For example, Gamboa-Santos et al. [131] designed an ultrasonic-assisted convective dryer for drying of strawberries. The prototype was initially a current pilot-scale convective dryer, with its drying chamber subsequently with an ultrasonic vibration system which included a cylindrical vibrating radiator driven by a piezoelectric transducer with the frequency of 21.8 kHz. Another similar dryer design using ultrasound for drying enhancement was described by Cruz et al. [133]. This equipment was a laboratory scale dryer modified with power ultrasound, automatic control of the air temperature and velocity and the weighing system of the samples.

Table 3
Hybrid drying methods combined with power ultrasound.

Combineddrying method	Material	US conditions	Main results	Ref.[No.]/ Year
	Strawberry	UP: 30 W, 60 W UF: 21.8 kHz	Power ultrasonic is a promising technology to reduce the drying time needed for heat sensitive products, such as strawberry	Ref. [131]/ 2014
	Loboapples	UP: 200 W UF: 26 kHz	Ultrasound enhances the drying efficiency of biological products without significantly raising their temperature.	Ref. [132]/ 2015
	Grape pomace	UP: 45 W UF: 21.7 kHz	Ultrasound application reduced the antioxidant potential due to oxidase activation and cell degradation.	Ref. [133]/ 2016
	Green pepper	UP: 100 W, 200 W UF: not reported	The effects of ultrasound on convective drying were assessed by “heating effect”, “vibration effect” and “synergistic effect”.	Ref. [134]/ 2017
	Garlic slices	UI: 216.8, 902.7 and 1513.5 W/m^2 UF: 20 kHz	Compared with non-ultrasound treated samples, the drying time of garlic samples sonicated at 1513.5 W/m2 was shortened by 35.0% at 50 °C, 48.5% at 60 °C and 50.0% at 70 °C.	Ref. [135]/ 2018
	Rough rice	UP: 30 W, 60, 90, 120, and 150 W UF: 21 kHz	Ultrasound assistance significantly increased bed evaporation rate up to 38.93%, and it caused a reasonable reduction in total drying time, energy consumption and broken kernel.	Ref. [136]/ 2018
	Cabbage	UP: 492.3,1131.1 W/m^2 UF: 20 kHz	Although both blanching and contacting sonication shortened the drying time, the losses of phenolics, glucosinolates and resulting breakdown products were not alleviated.	Ref. [137]/ 2019
Microwave-convective drying	Strawberry	UP: 100 W, 200 W UF: not reported	The ‘synergistic effect’ of microwaves and ultrasound improves the efficiency of heat and mass transfer in strawberries.	Ref. [138]/ 2016
	Carrot	UP: 75, 125 and 200 W UF: 26 kHz	Application of ultrasound and microwave in convective drying reduced drying time in the range of 9–81%.	Ref. [139]/ 2018
	Potato	UP: not reported UF: 40 kHz Operation time: 10, 20 and 30 min	The highest reduction in moisture content was observed in the samples pretreated with ultrasound for 10 min and then dried at 900 W microwave with the pulse ratio of 4.	Ref. [140]/ 2019
Vacuum drying	Beef and chicken meats	UP: 590 W UF: 40 kHz	The ultrasound-vacuum drying technique obviously shortened the drying period of beef and chicken.	Ref. [141]/ 2014
	Fish fillets	UP: 210 W UF: 40 kHz	The ultrasonic vacuum drying technique could reduce the drying time of fish fillets by 7.4–27.4% compared with vacuum-drying.	Ref. [142]/ 2015
	Carrot slices	UP: 200 W UF: 40 kHz	Compared with vacuum drying, the ultrasonic vacuum drying resulted in a 41–53% decrease in the drying time.	Ref. [143]/ 2016
	Potato strips	UP: 200 W UF: 40 kHz	Sonicated samples maintained mesophilic bacteria counts better than blanched and alginate coated vacuum-packaged potato strips.	Ref. [144]/ 2017
	Papaya	UP: 4870 W/m^2 UF: 25 kHz	Ultrasonic treatment accelerated the vacuum drying process for papaya and minimized the loss of the bioactive compounds studied and products' color.	Ref. [145]/ 2018
	Honey	UP:0.4,0.8,1.2,1.6 W/g UF: 28 kHz	The ultrasound enhanced vacuum drying of honey could be divided into two periods, namely accelerating rate period and falling rate period.	Ref. [146]/ 2019
	Nectarine	UP: 4870 W/m^2 UF: 25 kHz	Effective moisture diffusivity for ultrasound-assisted vacuum drying of nectarine was higher than 10^{-9} m^2/s.	Ref. [147]/ 2019
	Apple	UP: 10.3, 20.5 and 30.8 kW/m^3 UF: 25 kHz	The effective diffusion coefficient was 4.8 times higher after ultrasound with the power of 10.3 kW/m^3 was applied to the atmospheric freeze drying.	Ref. [148]/ 2015
	Apple	UP: 25, 50 and 75 W UF: 22 kHz	The most relevant operating parameter affecting the drying time of apple was the applied ultrasound power level in the atmospheric freeze drying assisted by power ultrasound.	Ref. [149]/ 2015
	Pear	UP:360 ,600 and 960 W UF: 20 kHz	Ultrasound pretreatment prior to freeze drying can improve the stability during storage of freeze dried pear.	Ref. [150]/ 2015
	Eggplant	UP: 25, 50 W; UF: 21.9 kHz	The application of ultrasound did not produce significant effects on the antioxidant indicators considered, and a non-negligible temperature rise when acoustic power was applied.	Ref. [151]/ 2018
	Onion	UP: different amplitude levels (24.4–61 μm) UF: 20 kHz	The ultrasound treatment improved the retention of bioactive compounds, and blanched and ultrasound treated dried onions exhibited similar color change.	Ref. [152]/ 2018
	Barley grass	UP: 10, 30, 45, 60 W/L; UF: 20 kHz	Ultra-sonication is an alternative to improve quality, flavor and energy consumption of barley grass in freeze drying.	Ref. [153]/ 2019

3.3. For welding

The ultrasonic vibration assisted welding is found to be more promising in improving the weld mechanical properties and microstructure due to nonlinear effects of power ultrasound including cavitation and acoustic flow in the molten pool. The acoustic waves produce tensile stresses in the rarefaction phase and causes cavitation in the liquid metal. The cavities result in high-intensity shock waves and intense convection in the molten pool. Acoustic flow is a type of turbulent flow that develops near the solid–liquid interface of the molten pool due to sound waves, which promotes the mixing of the base metal with the filler material and eliminates the partially diluted zone along the fusion line, thus increasing the resistance to corrosion in the material [154]. Moreover, the nonlinear effects induced by the ultrasound in the molten pool cause locally high-temperature and high-pressure regions, which might affect the solidification process greatly.

In order to enhance the mechanical properties of weld by using ultrasonic vibration, a new method of twin-arc TIG welding was developed by Wang et al. [155]. The welding method adopted combined ultrasonic arc and ordinary DC arc technology. The ultrasonic arc was used for injecting ultrasound excitation into the molten pool to improve weld quality, and the DC arc was used as main heat source to increase deposition efficiency. The method has been proved to thin the microstructure of weld and improve tensile properties of the weld effectively.

Dong et al. [156] used ultrasonic vibrations to weld high-strength aluminium alloy during gas-tungsten arc welding (GTAW) process. As shown in Fig. 19, an ultrasonic probe with 28 mm in diameter was placed 30 mm away from the weld pool, and the working frequency was

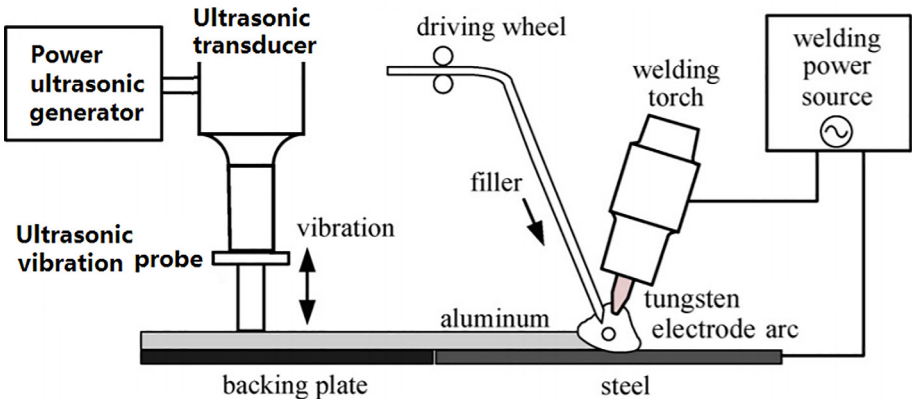

Fig. 19. Ultrasonic-vibration-assisted gas tungsten arc welding process [156].

20 kHz. Their study manifested that the ultrasonic vibration brought about grain refinement, decreased Fe–Al intermetallics, and increased microhardness in both the heat-affected zone and the weld, and as a result, it increased the joint strength by 27% during the GTAW process. Qi et al. [157] performed a study on the arc behavior by ultrasonic pulse GTAW process in the welding of stainless steel 0Cr18Ni9Ti and found that the increasing ultrasonic pulse frequency led to an obvious pinch effect of arc plasma and an increment of arc voltage, stiffness, and force.

The exerted ultrasonic vibration causes reduction in traverse force, tool torque and axial force of welding. According to the study by Zhong et al. [158], ultrasonic vibrations improved weld formation by either reducing or eliminating the weld defects, and the mechanical coupling between ultrasonic vibration and tool action was the main factor affecting both the welding process effectiveness and the joint quality in friction stir welding (FSW). To investigate the effect of ultrasonic vibrations on the CFSW of AZ31B Mg and 6061 Al alloys, an ultrasonic vibration set up (See Fig. 20) working under 20 kHz and ~25 μm amplitude has been designed by Kumar et al. [159]. Their study manifested that the ultrasonic vibrations induced additional turbulence in the stirred zone of the weldment which caused intense plastic deformation and resulted in a significant reduction in the magnitude of the axial force and tool torque during the friction stir welding. Moreover, the ultrasonic vibrations helped to reduce the defects in the weld nugget zone and hence improve the strength of welded joints.

The power ultrasonic can be also potentially used for thermoplastic composites welding [160,161]. Normally, the ultrasonic welding process could be divided into five steps: (1) mechanics and vibrations of the parts, (2) heat generation, (3) heat transfer, (4) flow and wetting, and (5) intermolecular diffusion [162]. The bonding mechanism for ultrasonically welded thermoplastic composites is the heating effect of power ultrasonic. The study on the bonding formation of the carbon fiber reinforced composite indicated that the bonding efficiency and weld area increased with an increase in welding energy until they reached a threshold after which the bonding efficiency would decrease due to material degradation as pores develop, but weld area would remain unchanged [162].

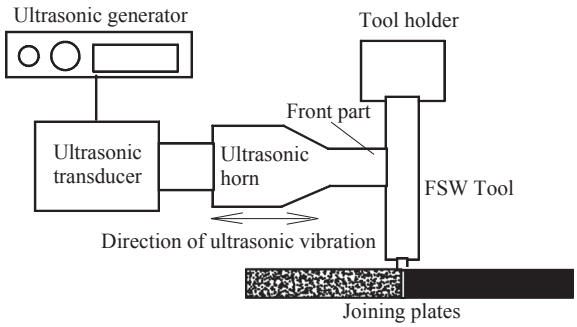

Fig. 20. Schematic of ultrasonic-assisted friction stir welding (FSW) [159].

In summary, ultrasonic vibrations will yield good results during metal welding in terms of improved mechanical properties, adept surface quality, improved material flow, and uniform grain growth etc. The weld mechanisms for thermoplastic composites are quite different from that for metal welding, i.e., the former mainly depends on intermolecular friction, and the latter mainly on interfacial friction. So, the ultrasonic heating is responsible for the thermoplastic composites welding. Several issues are still to be explored including the influence of the effects inherent in current oscillation at high frequencies on the dynamic response of the ultrasonic power, process optimization of complex vibration systems in ultrasonic forming and welding, optimized design of weld reed system as well as the development of technologically viable strategies for commercial implementation of this method.

3.4. For extraction

The cavitation effects of power ultrasound are considered as the main mechanisms of ultrasonic-assisted extraction. The physical process of ultrasonic cavitation, which is formed due to the continuous compression and rarefaction cycle of ultrasonic waves in the liquid, produces shear forces at the moment of bulb collapse and leads to cell wall destruction, particle size reduction and enhancement of mass transfer. Another important effect is that the ultrasonic cavitation can generate various types of free radicals. These radicals will participate in chemical processes and enhance the reaction rate [163].

In recent ten years, many researchers have managed to apply the power ultrasound to the bioactive compounds extraction from natural products including herb, plants, vegetables, fruits, and among others as listed in Table 4 [164–171]. It should be noted that different physical mechanisms were observed by studying extraction parameters. All these studies confirm that the power ultrasound surely intensify the extraction process, shorten the extraction time and increase yield of extracts. The acoustic power or intensity and frequency are important factors to be considered in the ultrasound-assisted extraction. For example, in the study by Zhang et al. [169], 40-kHz in the acoustic frequency was the most effective among the other frequencies (20, 28 and 60 kHz) for extraction of the peanut oil since it could obtain the desired cavitation effect.

As a novel, green and rapid developing technology, the ultrasonic-assisted extraction (UAE) is not only employed for improving the extraction efficiency of bioactive compounds, but also used as an effective instrument in separation science or industrial sector for evaluation of suitable sample mixture and particular concentration of the blend and extraction of nuclear like uranium [172]. Moreover, the power

Table 4
Applications of ultrasonic-assisted extraction.

Extract	Raw material	US conditions	Main results	Ref.[No.]/Year
Antioxidants	Pomegranate peel	UI: 59.2 W/ cm^2 UF: 20 kHz	Compared to conventional extract, pulsed ultrasound-assisted extraction at intensity level of 59.2 W/ cm^2, and the 5 and 5 s of pulse duration and interval increased the antioxidant yield by 22% and reduced the extraction time by 87%.	Ref. [164]/2011
Phenolic	Olive leaves	UP:160,240,320, 400 W UF: Not reported	Compared with conventional extraction, ultrasound assisted extraction reduced the extraction time from 24 h to 15 min and did not modify the extract composition.	Ref. [165]/2013
Polyphenols	Black tea	UP: 150 W UF: 25 kHz	The yield in the second maceration stage is about 13% higher for the two stage ultrasound maceration than for single stage ultrasound assisted extraction after conventional maceration.	Ref. [166]/2014
Phenolics and anthocyanins	Jabuticaba peel	UP: 150 W UF: 25 kHz	The effect of pH, ethanol concentration and extraction time were significant on ultrasound assisted extraction of phenolics and anthocyanin from jabuticaba peels.	Ref. [167]/2015
Pectin	'Tainong No. 1'mango peels	UP: 500 W UF: 20 kHz	Ultrasonic-assisted extraction reduced much more extraction time compared to the conventional extraction for comparable pectin yield.	Ref. [168]/2016
Oil	Peanut seeds	UP: 300 W UF: 20, 28, 40 and 60 kHz	The mechanism of ultrasonic cavitation on oil oxidation was studied. The best resonance frequency for the oil extraction was identified as 40 kHz according to the model results.	Ref. [169]/2017
Sodium hydroxide extracted proteins	Tea residue	UI: 377 W/L UF: 20 kHz	The thermodynamic properties comprising activation energy (Ea), change in enthalpy (DH) and entropy (DS) were reduced by ultrasound pretreatment whereas Gibbs free energy (DG) was increased.	Ref. [170]/2018
Phenolic compounds	Macela	UP: 100 W UF: 40 kHz	Ultrasound-assisted extraction increased the total phenolic compounds by 6.1-fold and the antioxidant activity by 3.4-fold compared with conventional extraction.	Ref. [171]/2018

ultrasound can be used for supercritical fluid extraction. Santos-Zea et al. [173] studied on the acoustic characterization of four transducers of different geometries and the evaluation of their performance in the ultrasonically assisted supercritical fluid extraction of antioxidants from oregano. It was found that transducer geometry influenced the amount and distribution of energy transmitted into the medium, thus determining the efficiency of the extraction process. Recently, Dassoff et al. [174] discussed mechanisms of ultrasound-assisted supercritical CO_2 extraction which are: i) Physical effects on the cell wall including enlargement of pores, cell damage, and increase in surface area; ii) Weakening of solute-matrix bonds; iii) Micro-mixing including movement of solute along wave front, vibrational friction and cell damage, and deposition of solute onto surface of particle; iv) Increased convective currents (macro-mixing). These mechanisms can be also used to describe the effects of ultrasound on extraction kinetics and to determine the effects of ultrasound under different operating conditions.

3.5. For heat transfer enhancement in liquid environment

Ultrasonic heat transfer enhancement is a well-known and highly effective approach of heat transfer enhancement and can be potentially applied to various industrial fields. Numerous studies [175–187] have been made to explore the process of ultrasonic heat transfer enhancement under different working conditions, as shown in Table 5.

For natural convection heat transfer in liquid environment, the ultrasonic 'cavitation' produces a bundle of jet-flow which is thought to enhance fluid mixing, reduce thermal boundary layer of the solid–liquid interface, suppress the formation of fouling, and hence increase convective heat transfer coefficient. Many recent studies have proved the positive effect of power ultrasound on convection heat transfer enhancement. Kiani et al. [175] studied the effect of ultrasound irradiation on the convective heat transfer rate during immersion cooling of a stationary sphere in an ethylene glycol–water mixture. Their study showed that the Nussle number (a dimensionless number of heat transfer) increased from about 23–27 to 25–108 depending on the ultrasonic intensity and the position of the sphere from the transducer surface. It was found that ultrasound not only increased heat transfer rates, but might also be a solution to fouling reduction. Fouling is considered to produce negative influence on the heat transfer of a heat exchanger. Chen et al. [177] conducted an experimental study to investigate antifouling effect of ultrasound to convective heat transfer process with cooling water as working fluid in different hardness and temperature. The experimental results of heat transfer process with ultrasonic treatment proved a remarkable effect of antifouling of power ultrasound. It was also found that the lower acoustic frequency would achieve the better antifouling effect than the higher acoustic frequency. In the other study by Hou et al. [180], the fouling process and antifouling effect in convective heat transfer under ultrasonic treatment with a frequency of 20.7 kHz and power ranging from 0 to 75 W were investigated. The experimental results showed that the fouling resistance with ultrasonic treatment decreased remarkably compared with the untreated case, and the fouling inhibition efficiency with ultrasonic treatment varied from 11.3% to 83.7% based on conditions of temperature and initial hardness.

The other aspect of ultrasonic waves is the effect on subcooled boiling. There are several mechanisms of power ultrasound for heat transfer enhancement under subcooled boiling conditions. Firstly, the cavitation bubbles can surely reduce the thickness of thermal boundary layer. Secondly, the acoustic streaming promotes the nucleation of boiling and the release of thermal bubbles from the surface of the heater which can carry away much heat. Thirdly, the acoustic streaming helps disengage the bubbles from the heat transfer surface, which prevents the vapor bubbles from aggregating on the surface. Bartoli et al. [183] carried out study on the ultrasonic heat transfer enhancement in subcooled boiling under a wide experimental conditions including various water subcooling degrees, ultrasonic power levels and frequency as well

Table 5
Heat transfer enhancement by power ultrasound.

Heat transfer mode	Medium	US conditions	Main results	Ref.[No.]/Year
	Ethylene glycol–water mixture	UI:120,190,450,890,1800,2800, 3400,4100 W m^2 UF:25 kHz	Ultrasound irradiation showed promising effect for the enhancement of convective heat transfer rate during immersion cooling. Enhancement factors from 1.02 to 4 were detected for different intensities and sphere locations.	Ref.[175]/ 2012
	Cheese milk	UP: 0–200 W UF: 20, 60, 150 kHz	Ultrasound can prevent biofouling in plate heat exchangers and can be used as a biofouling prevention technology suitable for use in the dairy industry.	Ref.[176]/ 2015
	Water	UP: 25–50 W UF: 28–40 kHz	Better antifouling effect could be achieved the lower frequency, and the higher antifouling rate was achieved with the higher power of ultrasound.	Ref.[177]/ 2016
	Water droplet	UI:100–2000 W/m^2 UP:20–80 kHz	Heat transfer was strengthened by mass transfer in the droplet freezing process. Comparing with no ultrasound, droplet temperature with ultrasound was lower 2.0 °C-2.5 °C for the same time.	Ref.[178]/ 2017
	Water	UP: 110 W UF: 2 MHz	Heat transfer coefficient under ultrasound remains constant while heat transfer coefficient under silent conditions increases with Reynolds number from 900 up to 5000.	Ref.[179]/ 2017
	Water	UP: 0–75 W UF: 20.7 kHz	Fouling inhibition efficiency with ultrasonic treatment varied from 11.3% to 83.7% based on conditions of temperature and initial hardness.	Ref.[180]/ 2018
	Water	UP: 150 W UF: 40 kHz	Heat transfer coefficient can increase up to 3880 W/m^2K and the enhancement ratio can reach up to 284% by ultrasonic vibration under a subcooled pool condition.	Ref.[181]/ 2018
	Water	UP: not reported UF: 25 kHz,2 MHz	High frequency ultrasound induces convective acoustic streaming while low frequency ultrasonic waves produce mainly cavitation effects. Thermal enhancement effect of acoustic streaming (2 MHz) decreases as flow rate increases, and it is the opposite for thermal enhancement effect produced by acoustic cavitation (25 kHz).	Ref.[182]/ 2019
Boiling	Water	UP:300 to 500 W UF:37,38, 39 and 40 kHz	The average percentage heat transfer enhancement started from 41% at 45 °C in subcooling degree, corresponding to 57% at 25 °C, and then started to decrease dramatically up to 15% at 10 °C.	Ref.[183]/ 2011
	Water	UP:300 to 500 W UF: 40 kHz	The enhancement of the heat transfer coefficient is lower than the one obtained in subcooled boiling and with regards to the saturated pool boiling conditions.	Ref.[184]/ 2012
	Degassed water	UP:30 to 90 W UF: 21, 45 kHz	The heat transfer enhancement is higher at frequency of 21 kHz than 45 kHz and that the ultrasonic power of 90 W results in a better cooling effect than that of 30 W.	Ref.[185]/ 2016
	Clean water and Alkyl Glucoside surfactant solutions	UP: not reported UF: 40 kHz	For boiling on the wire of d = 50 μm in subcooled water, enhancement of heat transfer coefficient due to ultrasonic is about 70% and 20% at heat flux q = 620 and 1350 kW/m^2, respectively. For boiling in surfactant solutions, the enhancement is 5–10% at q = 620 and 10–16% at q = 1350 kW/m^2 depending on solution concentration. For boiling on the tube of d = 1.5 mm in subcooled water, the enhancement is about 50% and 45% at q = 500 and 2500 kW/m^2, respectively.	Ref.[186]/ 2016
	LiBr solution	UP: 30–90 W UF: 21–45 kHz	Heat transfer coefficient at 21 kHz was higher than that at 45 kHz, and the heat transfer enhancement increased as the ultrasonic power rose from 30 to 90 W.	Ref.[187]/ 2016

as positions of the heater inside the ultrasonic tank. The results obtained with ultrasounds showed that the boiling heat transfer enhancement could increase by over 50% for specific conditions. Li et al. [185,187] reported the heat transfer enhancement due to ultrasonic vibration on horizontal copper tubes with different surface characteristics including smooth tube, screwed tube and finned tube in a subcooled boiling regime. The experimental results showed that the heat transfer enhancement was higher at 21 kHz than that at 45 kHz, and the heat transfer enhancement by ultrasound was more significant for the tubes with surface structures than that for the tube with smooth surface. Mosyak et al. [186] made an experimental study on the ultrasonic enhancement of heat transfer from the wire of d = 50 μm and the tube of d = 1.5 mm in subcooled pool boiling of clean water and Alkyl (8–16) Glucoside surfactant solutions of different concentrations. The enhancement of heat transfer brought by ultrasound was found to be closely related to the heat flux for boiling on the wire of d = 50 μm, while the heat flux produced small influence on the heat flux for boiling on the tube of d = 1.5 mm.

In summary, the current methods and approaches to obtain better ultrasonic heat transfer enhancement mainly include optimizing the ultrasonic parameters, changing surface structure, position of sound source or heater and liquid temperature as well as heat flux.

3.6. For other applications

Other applications of power ultrasound (as listed in Table 6) include but not limited to: de-ice, enhanced oil recovery, droplet atomization, cleaning and fine particle removal.

3.6.1. De-ice

Icing on the blade surfaces of wind turbines is a serious problem in cold regions, which greatly affects its performance. Compared with the conventional anti-icing and de-icing systems based on heating, the ultrasonic anti-icing/de-icing technique is considered to be energy saving. Since the adhesive bond of ice-substrate interface is relatively weak in shear strength compared with the interface forces within composite blades, ultrasonic piezoelectric actuators can produce high frequency vibrations and local shears at the locations of ice accretion to weaken the interface and subsequently deice the surface with normal impulse forces.

So far, no mature ultrasonic anti-icing and de-icing equipment development has been reported yet. This technique is still in laboratory research stage. For example, Wang et al. [188] designed a lithium niobate transducer for wind turbine blades de-icing and studied optimal acoustic frequency. Their study showed that the lithium niobate transducer could remove effectively the ice layer created in a freezer at −15 °C on the outer surface of wind turbine blade sample. Yin et al. [189] performed theoretic and experimental study on the PZT-5 piezoelectric transducers for wind turbine blade de-icing and discussed the installation way of ultrasonic transducers on the inner surface of wind turbine blade. Zeng et al. [190] also proved that 2 mm thick ice layer on an aluminum alloy plate and composite plate could be debonded quickly by using two smaller sandwich transducers in less than a minute through experimental study. Wang et al. [191] proposed a systematic method for the assessment and prediction of the effect of ultrasonic de-icing on composite wind turbine blades. The method could be used to determine the time consumption and the detaching process of the ice layer. In addition, they summarized recent developments related to ultrasonic guided wave (UGW) de-icing technologies used in aircraft icing including ultrasonic wave de-icing theory, advances in piezoelectric materials and transducers and novel devices designed for de-icing systems [192].

3.6.2. Enhanced oil recovery

Ultrasonic oil production technique is one of the most promising wave methods for improving the efficiency of enhanced oil recovery, which has several potential merits including high adaptability, simple operation, low cost and no pollution to environment. The effects of ultrasound on the well and the reservoir, which leads to enhanced production, mainly include preventing paraffin precipitation by ultrasonic wave, ultrasonic crude oil viscosity reduction, ultrasonic demulsification/dehydration, ultrasonic plugging removal, ultrasonic descaling/ anti-scaling [193]. Huang et al. [196] studied the mechanism of viscosity reduction due to ultrasonic waves by applying Fourier transform infrared spectrometer and analyzed viscosity reduction rule of residual oil by using Response Surface Method under conditions of changing ultrasonic exposure time, power and action mode. The results can provide data reference for the application of ultrasonic in the field of viscosity reduction for residual oil. Wang et al. [194] developed lithium niobate ultrasonic transducer for enhanced oil recovery and gave the optimum ultrasonic parameters for reducing the viscosity of super heavy oil. In the future, developing new ultrasonic

Table 6
Other applications for power ultrasound.

Application field	Environmental medium	Fundamental theory	Ref.[No.] /Year
De-ice	Solid	Ultrasonic piezoelectric actuators can produce high frequency vibrations (mechanical effect) and local shears at the locations of ice accretion to weaken the interface and subsequently deice the surface with normal impulse forces.	Ref.[188,189]/2016 Ref.[190,191]/2017 Ref.[192]/2018
Enhanced Oil Recovery	Liquid	Crude oil viscosity can be reduced by ultrasound. Paraffin crystallization process can be affected by ultrasonic excitation. The diameter of paraffin crystalline particles can get smaller due to ultrasound, which is conducive to improve the fluidity of crude oil.	Ref. [193]/2015 Ref. [194]/2017 Ref. [195,196]/2018
Dropletatomization	Liquid	Ultrasonic excitation generates capillary waves at the liquid–gas interface, which results in pinch-off of droplets from the wave peaks. As ultrasound waves propagate through the liquid phase, local pressure of the fluid drops below the vapor pressure leading to the formation of vapor bubbles. During the compression phase, these cavitation bubbles implode violently and emit hydraulic shocks which rupture the liquid–gas interface causing atomization.	Ref. [197]/2008 Ref. [198]/2012 Ref. [199]/2013 Ref. [205]/2016 Ref. [203,206]/2017 Ref. [200,201,204] /2018 Ref. [202]/2019
Cleaning	Liquid	Ultrasonic cleaning uses high-frequency, high-intensity sound waves in a liquid to facilitate or enhance the removal of foreign contaminants from surfaces submerged in an ultrasonically activated liquid. Clean a submerged component by the generation and implosion of cavitation bubbles on the fouled surface.	Ref. [207,208]/2016 Ref. [209]/2018
Fine particle removal	Gas	Orthokinetic and hydrodynamic interactions are the predominant mechanisms, while other effects, such as radiation force, acoustic streaming, and turbulence, can play an important role in promoting these interactions.	Ref. [210]/2013 Ref. [211]/2014 Ref. [212]/2011 Ref. [213,214]/2016 Ref. [215]/2018

transducer with excellent performance for enhanced oil recovery is an important research aspect [195].

3.6.3. Droplet atomization

Ultrasonic atomisers are based on the piezoelectric effect within ultrasonic horns, which can form ultrasonic atomization by vibrating a liquid layer with a piezoelectric crystal at high frequency (usually in the 50 kHz to 3 MHz range). Basically, the ultrasonic atomization can be explained by the surface-wave theory and the cavitation theory. Through studying thin-film nebulization mediated by surface acoustic-waves, Yeo et al. [197,198] concluded that the ultrasonic atomization was a result of surface-wave breakup. While according to the cavitation theory, the mechanism of ultrasonic atomization is that local pressure of the fluid drops below the vapor pressure leading to the formation of vapor bubbles during the propagation of ultrasonic waves in the liquid phase, and these cavitation bubbles implode violently and emit hydraulic shocks which rupture the liquid–gas interface causing atomization. An experimental study by Ramisetty et al. [199] reported the observation of a cavitation cloud in a droplet that was pendant from the face of an ultrasonic horn. Their results suggested that both the mechanisms should simultaneously responsible for the ultrasonic atomization. In a recent study by Deepu et al. [200], experiments were carried out on ultrasonic atomization of droplets at excitation frequency of f = 1.6 MHz to provide insight into the dynamics of ultrasonic atomization. A theoretical model was developed to predict the atomization life time of parent droplet based on the premise that capillary wave mechanism be responsible for droplet formation.

Atomization of liquids is important in many industrial processes, including spray drying [201,202], film coating[203,204], incineration and combustion of liquid fuel [205], making emulsions (sometimes nano-emulsions)[206], and etc. In most of these applications, droplets should have a required size distribution and a specific mean size. This is especially important for applications or products where the specific activity is or product characteristics are strongly dependent on the size distribution obtained in the process.

3.6.4. Cleaning

Ultrasonic cleaning technology has more recently been used in surface conditioning. Nguyen et al [207] provided a green technology that could clean turbine engine oil filters effectively in ships using ultrasound, with ultrasonic devices having a frequency of 25 kHz and different powers of 300 W and 600 W, respectively. The effects of temperature, ultrasonic cleaning times, pressure losses through the oil filter, solvent washing, and ultrasonic power devices were investigated, and it was found that that the necessary ultrasonic time varied significantly depending on which solvent was used for washing. Choi et al. [208] proposed a novel washing scheme by combining the ultrasonic vibration with a conventional washing method utilizing kinetic energy of textiles. According to the study, the hybrid washing scheme achieved a markedly enhanced performance up to 15% in comparison with the conventional washing machine.

Ultrasound is often used in ultrasonic baths to clean a submerged component by the generation and implosion of cavitation bubbles on the fouled surface. However, this requires the submersion of the fouled structure and thus may require a halt to production. Large fouled structures such as pipelines may not be accommodated. To deal this problem, Lais et al [209] used a non-invasive method of fouling removal using power ultrasound. The technique itself is carried out by using tailored bespoke HPUTs which are attached directly to the outer wall of the structure (submerged/filled with liquid) of interest.

3.6.5. Fine particle removal

The application of a high-intensity acoustic field to an aerosol may lead to a coagulation process of the suspended particles that is known as acoustic or ultrasonic agglomeration which makes fine particles grow and accelerates dust precipitation. The fundamental principle of acoustic agglomeration can be illustrated as follows: the propagation of sound waves result in the relative motion of aerosol particles and increase the collision probability among particles; Once the particles collide with each other, the smaller particles will tend to grow into larger one, and the newly-formed particles continue to agglomerate with the others, which ultimately brings about a continuous growth of aerosol particles. It is generally admitted that the predominant mechanisms of are orthokinetic and hydrodynamic interactions. Other effects like radiation force, acoustic streaming, and turbulence may play an important role in promoting these interactions. Orthokinetic interaction happens between two or more suspended particles of different sizes when they are located within a distance approximately equal to the displacement amplitude of the sound field in the suspending medium. Due to the effect of inertial force, there will be a relative motion between different sizes of particles, which will result in collision and agglomeration among particles. Intense acoustic fields generate hydrodynamic forces that cause the particles to approach from separation distances much larger than their respective acoustic displacements. Hydrodynamic mechanism can be employed to explain the agglomeration of monodisperse particles [210,211] and long-distant particles when subjected to the hydrodynamic force. The acoustic wake effect (AWE) induced by the hydrodynamic force is the asymmetry of the slip-flow velocity field in the Oseen regime, which may play a significant role in the agglomeration of monodisperse and long-distant particles.

The main practical application of acoustic agglomeration is clearly industrial gas cleaning [212], which has been shown as a new dust removal technology especially suitable for the removal of fine particles (like PM 2.5 and PM 1.0) through increasing the size of submicron particles to a size that can be readily collected by electrical or inertial methods [213]. However, there are still a number of challenges for the acoustic agglomeration to practice in real situations. For example, very powerful and efficient sonic generators are required for the great volumes to be treated. Meanwhile, the sonic system has to be flexible in applying different frequencies according to the changing conditions like particle size which often changes during the process. Therefore, future studies should be focused on the development of high-intensity and high-efficiency ultrasonic transducers and generators, optimization of agglomeration chamber structures, adding agglomeration nuclei [214,215], and so on.

4. Conclusions

A review of the state-and-art of high-intensity ultrasound and its applications has been presented in this paper. To begin with, the current developments of two types of ultrasonic transducers, i.e., magnetostrictive and piezoelectric types are reviewed. MPTs for plate applications can generate directional or omni-directional Lamb and shear-horizontal (SH) waves, while those for cylindrical waveguides can generate any type of wave mode, particularly the high-power torsional wave modes which would be difficult or cost-ineffective with other transducers. MPTs have some highlighted advantages like good sensitivity, durability, long-range inspection, easy implementation, cost-effectiveness and the capability to generate high-powered shear- or torsional-wave modes. However, there are also challenges in MPTs, for example, it is difficult to concentrate sufficiently strong magnetic fields on the magnetostrictive patches of MPTs; the transduction efficiency of MPTs can be poor at higher frequencies (over 1 MHz) due to internal wave reflection or ringing within a magnetostrictive patch. Another major issue with the magnetostrictive transducer is the large electrical energy dissipation in the form of heat which needs extra cost and weight of cooling system. As dynamic mechanical deformations in magnetostrictive patches generate elastic waves in waveguides, it is necessary to make a deep study on dispersion characteristics of waveguides induced by a MPT. Compared with the magnetostrictive ultrasonic transducer, the piezoelectric one has merits such as simple

structure, no electromagnetic radiation, high energy density, low cost and so on. For this reason, this paper particularly reports the current developments on piezoelectric transducers in terms of various vibrational modes for different practical aims. These include longitudinal mode, radial mode, flexural (or bending) mode, torsional mode and composite vibration modes like longitudinal-flexural, torsional-flexural and longitudinal-torsional.

Meanwhile, this paper also reviews recent studies on the applications of high-intensity ultrasound which are considered as new processes in fluids and multiphase media. These include processes such as chemical reactions, drying/dehydration, welding, extraction, heat transfer enhancement, de-ice, enhanced oil recovery, droplet atomization, cleaning and fine particle removal. It indicates that the applications of high-intensity ultrasound are an expanding diverse field with a broad and varied range of applications which cannot be all covered in this paper. All of these recent studies show that the high-intensity ultrasound can be considered to be one of the new environmentally friendly and energy-saving technologies. For example, the introduction of high-intensity ultrasound to the drying process can increase the drying rate and reduce the drying time significantly, which improves the energy efficiency of the process and lowers energy consumption.

The factors that appear to hinder large-scale applications of high-intensity ultrasound include competition from other less expensive methods, scale-up problems and general lack of information for the proposed application. In order to promote the future applications of ultrasonic technology, it is essential to have a good knowledge of each specific industrial problem prior to the development of optimal ultrasonic solutions. In addition, it is very critical to design and develop efficient power ultrasonic systems (generators and reactors) which can be adaptive to each specific industrial process. For the circumstance of fluid and gas media, the development of the stepped plate transducers with extensive radiating surface has promoted the implementation of high-intensity ultrasound to semi-industrial and industrial stages such as chemical reactions, drying, extraction, heat transfer enhancement, cleaning, enhanced oil recovery and so on. Although many published studies only considered the laboratory-scale solutions, attempts of large scale application were frequently reported. The effective use of high-intensity ultrasound in various industrial processes will see its bright future.

Acknowledgement

This work was supported by the National Natural Science Foundation of China under contract No. 11874326

Appendix A. Supplementary data

Supplementary data to this article can be found online at https://doi.org/10.1016/j.ultsonch.2019.104722.

References

[1] G. Wiedemann, Magnetische Untersuchungen, Ann. Phys. 193 (10) (1862) 193–217.
[2] D.C. Jiles, Theory of the magnetomechanical effect, J. Phys. D Appl. Phys. 28 (8) (1999) 1537–1546.
[3] J.D. Verhoeven, J.E. Ostenson, E.D. Gibson, O.D. McMasters, The effect of composition and magnetic heat treatment on the magnetostriction of TbxDy-xFey twinned single crystals, J. Appl. Phys. 66 (2) (1989) 772–779.
[4] W. Liu, L. Zhou, T. Xia, H. Yu, Rare earth ultrasonic transducer technique research, Ultrasonics 44 (Suppl 1) (2006) 689–692.
[5] A.G. Olabi, A. Grunwald, Design and application of magnetostrictive materials, Mater. Des. 29 (2) (2008) 469–483.
[6] J. Kim, E. Jung, Finite element analysis for acoustic characteristics of a magnetostrictive transducer, Smart Mater. Struct. 14 (6) (2005) 1273–1280.
[7] S. Valadkhan, K. Morris, A. Khajepour, Review and comparison of hysteresis models for magnetostrictive materials, J. Intell. Mater. Syst. Struct. 20 (1) (2009) 131–142.
[8] K. Jin, Y. Kou, X.J. Zheng, A nonlinear magneto-thermo-elastic coupled hysteretic constitutive model for magnetostrictive alloys, J. Magn. Magn. Mater. 324 (12) (2012) 1954–1961.
[9] H. Xu, Y. Pei, D. Fang, S. Ai, An energy-based dynamic loss hysteresis model for giant magnetostrictive materials, Int. J. Solids Struct. 50 (5) (2013) 672–679.
[10] Z. Deng, Dynamic discrete energy-averaged model for magnetostrictive materials, J. Magn. Magn. Mater. 441 (11) (2017) 757–763.
[11] Y. Shi, Y. Gao, A quasistatic hysteresis model for magnetoelectric effect in multiferroic nanostructured films with surface effect, J. Alloy. Compd. 762 (9) (2018) 706–718.
[12] F. Stillesjo, G.Engdahl, Z.Wei. Dynamic simulation and performance study of magnetostrictive transducers for ultrasonic applications. Proc SPIE – The International Society for Optics and Photonics Engineering 2000, 3992, pp. 594–602.
[13] S.N. Jammalamadaka, G. Markandeyulu, E. Kannan, Development of a magetnetostrictive transducer for nondestructive testing of concrete structures, Appl. Phys. Lett. 92 (4) (2008) 531–1304.
[14] W. Huang, L. Zhai, B. Wang, Optimization design and dynamic analysis of giant magnetostrictive transducer based on finite element method, Int. J. Appl. Electromagnet. Mech. 33 (3) (2010) 953–959.
[15] G. Zeng, B. Cao, H. Zeng, Analysis of dynamic characteristics of the magnetostrictive power ultrasonic transducer, Appl. Mechan. Mater. 105–107 (2012) 1693–1696.
[16] F.T. Calkins, M.J. Dapino, A.B. Flatau, Effect of prestress on the dynamic performance of a Terfenol-D transducer, Proceed. Smart Struct. Mater. (1997) 3041–3123.
[17] M. Sheykholeslami, Y. Hojjat, M. Ghodsi, K. Kakavand, S. Cinquemani, Investigation ofΔE effect on vibrational behavior of giant magnetostrictive transducers, Shock Vib. 2015 (2015) 1–9.
[18] M.R. Sheykholeslami, Y. Hojjat, S. Cinquemani, M. Ghodsi, M. Karafi, An approach to design and fabrication of resonant giant magnetostrictive transducer, Smart Struct. Syst. 17 (2) (2016) 313–325.
[19] M.R. Karafi, M. Ghodsi, Y. Hojjat, Development of magnetostrictive resonant torsional vibrator, IEEE Trans. Magn. 51 (9) (2015) 1–8.
[20] M.R. Karafi, Y. Hojjat, F. Sassani, M. Ghodsi, A novel magnetostrictive torsional resonant transducer, Sens. Actuators, A 195 (2) (2013) 71–78.
[21] P. Li, Q. Liu, S. Li, Q. Wang, D. Zhang, Y. Li, Design and numerical simulation of novel giant magnetostrictive ultrasonic transducer, Results Phys. 7 (2017) 3946–3954.
[22] W. Huang, Y. Li, L. Weng, Multifield coupling model with dynamic losses for giant magnetostrictive transducer, IEEE Trans. Appl. Supercond. 26 (4) (2016) 4900805.
[23] Y. Wu, J. Xu, Research on methods of thermal error compensating and restraining in giant magnetostrictive actuator, J. Eng. Des. 12 (4) (2005) 213–218.
[24] Y. Jia, J. Tan, Study on micro-position actuator system of giant magnetostriction materials, Chinese J. Scient. Instrum. 1 (2000) 38–41.
[25] Q. Lu, C. Jing, Z. Min. Integrated optimized design of GMA with doublewater-cooling cavums, in: International Conference on Mechanic Automationand Control Engineering (MACE), June, 2010, 3562–3565.
[26] Y.K. Kwak, S.H. Kim, J.H. Ahn, Improvement of positioning accuracy of magnetostrictive actuator by means of built-in air cooling and temperature control, Int. J. Precis. Eng. Manuf. 12 (5) (2011) 829–834.
[27] J. Xu, Y. Wu, Z. Zhao, R. Ge, The design of temperature control system in giant magnetostrictive actuator, Modular Mach. Tool Autom. Manufact. Techn. 10 (2007) 47–49.
[28] Y. Zhu, L. Ji, Theoretical and experimental investigations of the temperature and thermal deformation of a giant magnetostrictive actuator, Sens. Actuators, A 218 (10) (2014) 167–178.
[29] M.S. Choi, S.Y. Kim, H. Kwun, An equivalent circuit model of magnetostrictive transducers for guided wave applications, J. Kor. Phys. Soc. 47 (3) (2005) 454–462.
[30] R. Ribichini, F. Cegla, P.B. Nagy, P. Cawley, Quantitative modeling of the transduction of electromagnetic acoustic transducers operating on ferromagnetic media, IEEE Trans. Ultrason. Ferroelect. Frequ. Control 57 (12) (2010) 2808–2817.
[31] J.H. Oh, K.H. Sun, Y.Y. Kim, Time-harmonic finite element analysis of guided waves generated by magnetostrictive patch transducers, Smart Mater. Struct. 22 (8) (2013) 085007.
[32] Z. Liu, Y. Hu, J. Fan, W. Yin, C. He, B. Wu, Longitudinal mode magnetostrictive patch transducer array employing a multi-splitting meander coil for pipe inspection, NDT and E Int. 79 (4) (2015) 30–37.
[33] S.H. Cho, H.W. Kim, Y.Y. Kim, Megahertz-range guided pure torsional wave transduction and experiments using a magnetostrictive transducer, IEEE Trans. Ultrason. Ferroelect. Frequ. Cont. 57 (5) (2010) 1225–1229.
[34] H.W. Kim, S.H. Cho, Y.Y. Kim, Analysis of internal wave reflection within a magnetostrictive patch transducer for high-frequency guided torsional waves, Ultrasonics 51 (6) (2011) 647–652.
[35] H.W. Kim, Y.E. Kwon, J.K. Lee, Y.Y. Kim, Higher torsional mode suppression in a pipe for enhancing the first torsional mode by using magnetostrictive patch transducers, IEEE Trans. Ultrason. Ferroelect. Frequen. Control 60 (3) (2013) 562–572.
[36] Z. Liu, J. Fan, Y. Hu, C. He, B. Wu, Torsional mode magnetostrictive patch transducer array employing a modified planar solenoid array coil for pipe inspection, NDT E Int. 69 (1) (2015) 9–15.
[37] S.H. Cho, S.W. Han, C.I. Park, Y.Y. Kim, Noncontact torsional wave transduction in a rotating shaft using oblique magnetostrictive strips, J. Appl. Phys. 100 (10) (2006) 104903.
[38] T. Hayashi, M. Murase, Defect imaging with guided waves in a pipe, J. Acoust. Soc.

Am. 117 (4 Pt 1) (2005) 2134–2140.
[39] H.W. Kim, H.J. Lee, Y.Y. Kim, Health monitoring of axially-cracked pipes by using helically propagating shear-horizontal waves, NDT and E Int. 46 (1) (2012) 115–121.
[40] M. Clough, M. Fleming, S. Dixon, Circumferential guided wave EMAT system for pipeline screening using shear horizontal ultrasound, NDT and E Int. 86 (3) (2017) 20–27.
[41] H. Kwun, S.Y. Kim, G.M. Light, Long-range guided wave inspection of structures using the magnetostrictive sensor, J. Kor. Soc. Nondestruct. Test. 21 (2001) 383–390.
[42] S.H. Cho, J.S. Lee, Y.Y. Kim, Guided wave transduction experiment using a circular magnetostrictive patch and a figure-of-eight coil in nonferromagnetic plates, Appl. Phys. Lett. 88 (22) (2006) 224101.
[43] J.S. Lee, S.H. Cho, Y.Y. Kim, Radiation pattern of Lamb waves generated by a circular magnetostrictive patch transducer, Appl. Phys. Lett. 90 (5) (2007) 054102.
[44] J.S. Lee, Y.Y. Kim, S.H. Cho, Beam-focused shear-horizontal wave generation in a plate by a circular magnetostrictive patch transducer employing a planar solenoid array, Smart Mater. Struct. 18 (1) (2009) 015009.
[45] L. Zhou, Y. Yang, F.-G. Yuan, Design of a magnetostrictive sensor for structural health monitoring of non-ferromagnetic plates, J. Vibroeng. 14 (1) (2012) 280–291.
[46] B. Yoo, S.-M. Na, A.B. Flatau, D.J. Pines, Directional magnetostrictive patch transducer based on Galfenol's anisotropic magnetostriction feature, Smart Mater. Struct. 23 (9) (2014) 095035.
[47] J.K. Lee, H.W. Kim, Y.Y. Kim, Omnidirectional Lamb waves by axisymmetrically-configured magnetostrictive patch transducer, IEEE Trans. Ultrason. Ferroelect. Frequ. Control 60 (9) (2013) 1928–1934.
[48] H.M. Seung, H.W. Kim, Y.Y. Kim, Development of an omni-directional shearhorizontal wave magnetostrictive patch transducer for plates, Ultrasonics 53 (7) (2013) 1304–1308.
[49] H.M. Seung, C.I. Park, Y.Y. Kim, An omnidirectional shear-horizontal guided wave EMAT for a metallic plate, Ultrasonics 69 (7) (2016) 58–66.
[50] Y.E. Kwon, H.J. Jeon, H.W. Kim, Y.Y. Kim, Waveguide tapering for beam-width control in a waveguide transducer, Ultrasonics 54 (3) (2014) 953–960.
[51] H. Kwun, S.Y. Kim, Magnetostrictive sensor for generating and detecting plate guided waves, J. Pressure Vessel Technol. 127 (3) (2005) 284–289.
[52] J.S. Lee, H.W. Kim, B.C. Jeon, S.H. Cho, Y.Y. Kim, Damage detection in a plate using beam-focused shear-horizontal wave magnetostrictive patch transducers, Aiaa J. 48 (3) (2012) 654–663.
[53] P.S. Ma, H.W. Kim, J.H. Oh, Y.Y. Kim, Mode separation of a single-frequency bimodal elastic wave pulse by a phononic crystal, Appl. Phys. Lett. 99 (20) (2011) 201906.
[54] J.H. Oh, H.W. Kim, P.S. Ma, H.M. Seung, Y.Y. Kim, Inverted bi-prism phononic crystals for one-sided elastic wave transmission applications, Appl. Phys. Lett. 100 (21) (2012) 213503.
[55] J.H. Oh, H.M. Seung, Y.Y. Kim, A truly hyperbolic elastic metamaterial lens, Appl. Phys. Lett. 104 (7) (2014) 073503.
[56] C. Liang, B. Prorok, Measuring the thin film elastic modulus with a magnetostrictive sensor, J. Micromech. Microeng. 17 (4) (2007) 709–716.
[57] E. Saidha, G.N. Naik, S. Gopalkrishnan, An experimental investigation of a smart laminated composite beam with a magnetostrictive patch for health monitoring applications, Struct. Health Monit. 2 (4) (2003) 273–292.
[58] D.P. Ghosh, S. Gopalakrishnan, Coupled analysis of composite laminate with embedded magnetostrictive patches, Smart Mater. Struct. 14 (6) (2005) 1462–1473.
[59] D.A. Wang, W.Y. Chuang, K. Hsu, H.T. Pham, Design of a Bezier-profile horn for high displacement amplification, Ultrasonics 51 (2) (2011) 148–156.
[60] H. Nguyen, H. Nguyen, J. Uan, D. Wang, A nonrational B-spline profiled horn with high displacement amplification for ultrasonic welding, Ultrasonics 54 (8) (2014) 2063–2071.
[61] M.R. Rani, R. Rudramoorthy, Computational modeling and experimental studies of the dynamic performance of ultrasonic horn profiles used in plastic welding, Ultrasonics 53 (3) (2013) 763–772.
[62] L. Xu, Investigation of a cup-shaped ultrasonic transducer operated in the full-wave vibrational mode, Ultrasonics 59 (5) (2015) 109–118.
[63] Q. Zhang, S. Shi, W. Chen, An electromechanical coupling model of a longitudinal vibration type piezoelectric ultrasonic transducer, Ceram. Int. 41 (7) (2015) S638–S644.
[64] J. Grabalosa, I. Ferrer, O. Martínez-Romero, A. Elías-Zúeniga, X. Planta, F. Rivillas, Assessing a stepped sonotrode in ultrasonic molding technology, J. Mater. Process. Technol. 229 (3) (2016) 687–696.
[65] S. Lin, H. Guo, J. Xu, Actively adjustable step-type ultrasonic horns in longitudinal vibration, J. Sound Vib. 419 (4) (2018) 367–379.
[66] M.K. Kurosawa, O. Kodaira, Y. Tsuchitoi, T. Higuchi, Transducer for high speed and large thrust ultrasonic linear motor using two sandwich-type vibrators, IEEE Trans. Ultrason. Ferroelectr. Freq. Control 45 (5) (1998) 1188–1195.
[67] R.C. Ibrahim, A novel linear piezoelectric motor with complex vibration modes, Ferroelectrics 338 (1) (2006) 65–72.
[68] K. Asumi, R. Fukunaga, T. Fujimura, M.K. Kurosawa, High speed, high resolution ultrasonic linear motor using V-shape two bolt-clamped Langevin-type transducers, Acoust. Sci. Technol. 30 (3) (2009) 180–186.
[69] K. Asumi, R. Fukunaga, T. Fujimura, M.K. Kurosawa, Miniaturization of a V-shape transducer ultrasonic motor, Jpn. J. Appl. Phys. 48 (7) (2009) 07GM02.
[70] A. Suzuki, M. Tsunoji, J. Tsujino, Characteristics of ultrasonic linear motor that incorporates two transducers at an acute angle, Jpn. J. Appl. Phys. 52 (7S) (2013) 07HE04.
[71] P. Guo, K.F. Ehmann, Development of a tertiary motion generator for elliptical vibration texturing, Precis. Eng. 37 (2) (2013) 364–371.
[72] X. Li, Z. Yao, Analytical modeling and experimental validation of a V-shape piezoelectric ultrasonic transducer, Smart Mater. Struct. 25 (7) (2016) 075026.
[73] L. Wang, V. Hofmann, F. Bai, J. Jin, J. Twiefel, A novel additive manufactured three-dimensional piezoelectric transducer: Systematic modeling and experimental validation, Mech. Syst. Sig. Process. 114 (1) (2019) 346–365.
[74] J.A. Gallego-Juárez, G. Rodriguez, V. Acosta, E. Riera, Power ultrasonic transducers with extensive radiators for industrial processing, Ultrason. Sonochem. 17 (6) (2010) 953–964.
[75] J. Ning, X. He, G. Zhao, Effects of driving frequency of longitudinal transducer on the vibration characteristics of a stepped plate, Appl. Acoust. 79 (4) (2014) 164–168.
[76] W. Xie, C. Fan, C. Yang, S. Lin, Effect of acoustic field parameters on arc acoustic binding during ultrasonic wave-assisted arc welding, Ultrason. Sonochem. 29 (3) (2016) 476–484.
[77] J. Wang, Q. Sun, J. Teng, P. Jin, T. Zhang, J. Feng, Enhanced arc-acoustic interaction by stepped-plate radiator in ultrasonic wave-assisted GTAW, J. Mater. Process. Techol. 262 (12) (2018) 19–31.
[78] X. Lu, J. Hu, H. Peng, Y. Wang, A new topological structure for the Langevin-type ultrasonic transducer, Ultrasonics 75 (3) (2017) 1–8.
[79] J.O. Kim, J.G. Lee, Dynamic characteristics of piezoelectric cylindrical transducers with radial polarization, J. Sound Vib. 300 (1–2) (2007) 241–249.
[80] S. Lin, Electro-mechanical equivalent circuit of a piezoelectric ceramic thin circular ring in radial vibration, Sens. Actuators, A 134 (2) (2007) 505–512.
[81] S. Lin, Study on the radial composite piezoelectric ceramic transducer in radial vibration, Ultrasonics 46 (1) (2007) 51–59.
[82] S.Y. Lin, S.J. Wang, Z.Q. Fu, Electro-mechanical equivalent circuit for the radial vibration of the radially poled piezoelectric ceramic long tubes with arbitrary wall thickness, Sens. Actuat., A 180 (6) (2012) 87–96.
[83] L.K. Wang, Y. Lu, Y. Xiang, L. Qin, D.K. Cai, Vibration analysis for piezoceramic ring, Ceram. Int. 39 (Supplement 1) (2013) S739–S742.
[84] T. Ye, G. Jin, S. Shi, X. Ma, Three-dimensional free vibration analysis of thick cylindrical shells with general end conditions and resting on elastic foundations, Int. J. Mech. Sci. 84 (7) (2014) 120–137.
[85] H.M. Wang, D.S. Luo, Exact analysis of radial vibration of functionally graded piezoelectric ring transducers resting on elastic foundation, Appl. Math. Model. 40 (4) (2016) 2549–2559.
[86] Y. Sunny, C.R. Bawiec, A.T. Nguyen, J.A. Samuels, M.S. Weingarten, L.A. Zubkov, P.A. Lewin, Optimization of un-tethered, low voltage, 20–100 kHz flexural transducers for biomedical ultrasonics applications, Ultrasonics 52 (9) (2012) 943–948.
[87] C.R. Bawiec, Y. Sunny, A.T. Nguyen, J.A. Samuels, M.S. Weingarten, L.A. Zubkov, P.A. Lewin, Finite element static displacement optimization of 20–100 kHz flexural transducers for fully portable ultrasound applicator, Ultrasonics 53 (2) (2013) 511–517.
[88] Q. Zhang, S. Shi, W. Chen, An electromechanical coupling model of a bending vibration type piezoelectric ultrasonic transducer, Ultrasonics 66 (3) (2016) 18–26.
[89] T.J.R. Eriksson, S.N. Ramadas, S.M. Dixon, Experimental and simulation characterisation of flexural vibration modes in unimorph ultrasound transducers, Ultrasonics 65 (2) (2016) 242–248.
[90] R. Yamamoto, D. Koyama, M. Matsukawa, On-chip ultrasonic manipulation of microparticles by using the flexural vibration of a glass substrate, Ultrasonics 79 (8) (2017) 81–86.
[91] L. Wang, V. Hofmannb, F. Bai, J. Jin, J. Yang Liu, Twiefel, Systematic electromechanical transfer matrix model of a novel sandwiched type flexural piezoelectric transducer, Int. J. Mech. Sci. 138–139 (4) (2018) 229–243.
[92] J.O. Kim, O.S. Kwon, Vibration characteristics of piezoelectric torsional transducers, J. Sound Vib. 264 (2) (2003) 453–473.
[93] T. Harada, N. Ishikawa, T. Kanda, K. Suzumori, Y. Yamada, K.I. Sotowa, Droplet generation using a torsional Langevin-type transducer and a micropore plate, Sens. Actuat., A 155 (10) (2009) 168–174.
[94] Y. Kiyama, Y. Tominaga, T. Kanda, K. Suzumori, T. Kishi, Y. Yamada, N. Seno, Evaluation of generated micro droplets using micropore plates oscillated by ultrasonic torsional transducers, Sens. Actuat., A 185 (10) (2012) 92–100.
[95] J.M. Chang, W.K. Moon, N. Cho, A. Yi, H.R. Koo, W. Han, D.Y. Noh, H.G. Moon, S.J. Kim, Clinical application of shear wave elastography (SWE) in the diagnosis of benign and malignant breast diseases, Breast Cancer Res. Treat. 129 (1) (2011) 89–97.
[96] J. Melchor, G. Rus, Torsional ultrasonic transducer computational design optimization, Ultrasonics 54 (9) (2014) 1950–1962.
[97] Y. Peng, Y. Peng, X. Gu, J. Wang, H. Yu, A review of long range piezoelectric motors using frequency leveraged method, Sens. Actuators, A 235 (11) (2015) 240–255.
[98] Y. Liu, W. Chen, J. Liu, S. Shi, A cylindrical traveling wave ultrasonic motor using longitudinal and bending composite transducer, Sens. Actuators, A 161 (1–2) (2010) 158–163.
[99] X. Yang, Y. Liu, W. Chen, J. Liu, Longitudinal and bending hybrid linear ultrasonic motor using bending PZT elements, Ceram. Int. 39 (5) (2013) S691–S694.
[100] Y. Liu, S. Shi, C. Li, W. Chen, J. Liu, A novel standing wave linear piezoelectric actuator using the longitudinal-bending coupling mode, Sens. Actuators, A 251 (11) (2016) 119–125.
[101] X. Yang, Y. Liu, S. Shi, W. Chen, X. Qi, Development of a novel ultrasonic drill using longitudinal-bending hybrid mode, IEEE Access 5 (2017) 7362–7370.

[102] L. Wang, V. Hofmann, F. Bai, Modeling of coupled longitudinal and bending vibrations in a sandwich type piezoelectric transducer utilizing the transfer matrix method, Mech. Syst. Sig. Process. 108 (8) (2018) 216–237.
[103] Q. Shen, Y. Liu, L. Wang, J. Liu, K. Li, A long stroke linear stepping piezoelectric actuator using two longitudinal-bending hybrid transducers, Ceram. Int. 44 (11) (2018) S104–S107.
[104] L. Wang, Y. Liu, K. Li, S. Chen, X. Tian, Development of a resonant type piezoelectric stepping motor using longitudinal and bending hybrid bolt-clamped transducer, Sens. Actuat., A 285 (1) (2019) 182–189.
[105] L. Wang, C. Xue, V. Hofmann, F. Bai, J. Jin, J. Twiefel, Semi-analytical modeling and optimization of a traveling wave sandwich piezoelectric transducer with a beam-ring combined structure, Mech. Syst. Sig. Process. 122 (5) (2019) 171–191.
[106] P. Harkness, M. Lucas, A. Cardoni, Coupling and degenerating modes in longitudinal–torsional step horns, Ultrasonics 52 (8) (2012) 980–988.
[107] H. Al-Budairi, M. Lucas, P. Harkness, A design approach for longitudinal-torsional ultrasonic transducers, Sens. Actuat., A 198 (8) (2013) 99–106.
[108] C. Yang, X. Shan, T. Xie, A new piezoelectric ceramic longitudinal–torsional composite ultrasonic vibrator for wire drawing, Ceram. Int. 41 (S1) (2015) S625–S630.
[109] S. Liu, X. Shan, W. Cao, Y. Yang, T. Xie, A longitudinal-torsional composite ultrasonic vibrator with thread grooves, Ceram. Int. 43 (8) (2017) S214–S220.
[110] D. Bai, Q. Quan, Y. Wang, D. Tang, Z. Deng, A longitudinal & longitudinal-torsional vibration actuator for rotary-percussive ultrasonic planetary drills, Adv. Space Res. 63 (2) (2019) 1065–1072.
[111] Y. Liu, J. Liu, W. Chen, A rotary ultrasonic motor using radial bending mode of ring with nested PZT excitation, J. Zhej. Univer.- Sci. A 13 (3) (2012) 189–196.
[112] W. Chen, Y. Liu, X. Yang, Ring-type traveling wave ultrasonic motor using a radial bending mode, IEEE Trans. Ultrason. Ferroelectr. Freq. Control 61 (1) (2014) 197–202.
[113] V. Singh, K.P. Kaur, A. Khurana, G.L. Kad, Ultrasound: a boon in the synthesis of organic compounds, Resonance 3 (9) (1998) 56–60.
[114] N. Her, J. Park, J. Oh, New design approaches for ultrasonic reactors: degradation of naphthalene and phenol in water, Water Air Soil Pollut. 220 (1–4) (2011) 173–180.
[115] H. Zeng, H. Li, H. Shao, One-pot three-component Mannich-type reactions using Sulfamic acid catalyst under ultrasound irradiation, Ultrason. Sonochem. 16 (3) (2009) 758–762.
[116] D. Bandyopadhyay, S. Mukherjee, L.C. Turrubiartes, Ultrasound-assisted aza-Michael reaction in water: A green procedure, Ultrason. Sonochem. 19 (4) (2012) 969–973.
[117] C.E. Domini, G.F. Silbestri, B. Fernández Band, A.B. Chopa, B.F. Band, Ultrasound-assisted synthesis of unsymmetrical biaryls by Stille cross-coupling reactions, Ultrason. Sonochem. 19 (3) (2012) 410–414.
[118] G. Chatel, C. Monnier, N. Kardos, C. Voiron, B. Andrioletti, M. Draye, Green, selective and swift oxidation of cyclic alcohols to corresponding ketones, Appl. Catal. A 478 (2014) 157–164.
[119] D. Li, J. Song, A. Xu, C. Liu, Optimization of the ultrasound-assisted synthesis of lutein disuccinate using uniform design, Ultrason. Sonochem. 21 (1) (2014) 98–103.
[120] K. Harikumar, V. Rajendran, Ultrasound assisted the preparation of 1-butoxy-4-nitrobenzene under a new multi-site phase-transfer catalyst – Kinetic study, Ultrason. Sonochem. 21 (1) (2014) 208–215.
[121] G.V. Waghmare, M.D. Vetal, V.K. Rathod, Ultrasound assisted enzyme catalyzed synthesis of glycerol carbonate from glycerol and dimethyl carbonate, Ultrason. Sonochem. 22 (2) (2015) 311–316.
[122] M.C. Diwathe, P.R. Gogate, Ultrasound assisted intensified synthesis of 1-benzyloxy-4-nitrobenzene in the presence of phase transfer catalyst, Chem. Eng. J. 346 (8) (2018) 438–446.
[123] R. Mathiarasi, N. Partha, Optimization, kinetics and thermodynamic studies on oil extraction from Daturametel Linn oil seed for biodiesel production, Renew. Energy 96 (10) (2016) 583–590.
[124] S.D. Ali, I.N. Javed, U.A. Rana, M.F. Nazar, Novel SrO-CaO Mixed metal oxides catalyst for ultrasonic-assisted transesterification of jatropha oil into Biodiesel, Austr. J. Chem. 70 (3) (2016) 258.
[125] P.B. Subhedar, P.R. Gogate, Ultrasound assisted intensification of biodiesel production using enzymatic interesterification, Ultrason. Sonochem. 29 (1) (2016) 67–75.
[126] A. Nikseresht, A. Daniyali, M. Ali-Mohammadi, A. Afzalinia, A. Mirzaie, Ultrasound-assisted biodiesel production by a novel composite of Fe(III)-based MOF and phosphotangestic acid as efficient and reusable catalyst, Ultrason. Sonochem. 37 (7) (2017) 203–207.
[127] Y. Liu, D. Jin, X. Lu, P. Han, Study on degradation of dimethoate solution in ultrasonic airlift loop reactor, Ultrason. Sonochem. 15 (5) (2008) 755–760.
[128] Y. Asakura, K. Yasuda, D. Kato, Y. Kojima, S. Koda, Development of a large sonochemical reactor at a high frequency, Chem. Eng. J. 139 (2) (2008) 339–343.
[129] J. Safari, L. Javadian, Ultrasound assisted the green synthesis of 2-amino-4H chromene derivatives catalyzed by Fe3O4-functionalized nanoparticles with chitosan as a novel and reusable magnetic catalyst, Ultrason. Sonochem. 22 (3) (2015) 341–348.
[130] A. Francony, C. Petrier, Sonochemical degradation of carbon tetrachloride in aqueous solution at two frequencies: 20 kHz and 500 kHz, Ultrason. Sonochem. 3 (2) (1996) S77–S82.
[131] J. Gamboa-Santos, A. Montilla, J.A. Cárcel, M. Villamiel, J.V. García-Pérez, Air-borne ultrasound application in the convective drying of strawberry, J. Food Eng. 128 (5) (2014) 132–139.
[132] S.J. Kowalski, A. Pawłowski, Intensification of apple drying due to ultrasound enhancement, J. Food Eng. 156 (7) (2015) 1–9.
[133] L. Cruz, G. Clemente, A. Mulet, M.H. Ahmad-Qasem, E. Barrajón-Catalán, J.V. García-Pérez, Air-borne ultrasonic application in the drying of grape skin: kinetic and quality considerations, J. Food Eng. 168 (1) (2016) 251–258.
[134] J. Szadzińska, J. Łechtańska, S.J. Kowalski, M. Stasiak, The effect of high power airborne ultrasound and microwaves on convective drying effectiveness and quality of green pepper, Ultrason. Sonochem. 34 (1) (2017) 531–539.
[135] Y. Tao, J. Zhang, S. Jiang, Y. Xu, M. Ye, Contacting ultrasound enhanced hot-air convective drying of garlic slices: Mass transfer modeling and quality evaluation, J. Food Eng. 235 (10) (2018) 79–88.
[136] N. Dibagar, R.A. Chayjan, S.J. Kowalski, S.H. Peyman, Deep bed rough rice air-drying assisted with airborne ultrasound set at 21 kHz frequency: A physico-chemical investigation and optimization, Ultrason. Sonochem. 53 (5) (2019) 25–43.
[137] Y. Tao, M. Han, X. Gao, Y. Han, G. Xie, Applications of water blanching, surface contacting ultrasound-assisted airdrying, and their combination for dehydration of white cabbage: Dryingmechanism, bioactive profile, color and rehydration property, Ultrason. Sonochem. 53 (5) (2019) 192–201.
[138] J. Szadzińska, S.J. Kowalski, M. Stasiak, Microwave and ultrasound enhancement of convective drying of strawberries: Experimental and modeling efficiency, Int. J. Heat Mass Transf. 103 (12) (2016) 1065–1074.
[139] J. Kroehnke, J. Szadzińska, M. Stasiak, E. Radziejewska-Kubzdela, G. Musielak, Ultrasound- and microwave-assisted convective drying of carrots – Process kinetics and product's quality analysis, Ultrason. Sonochem. 48 (11) (2018) 249–258.
[140] J. Dehghannya, S. Kadkhodaei, M.K.Heshmati. Ultrasound-assisted intensification of a hybrid intermittent microwave – hot air drying process of potato: Quality aspects and energy consumption. Ultrasonics, doi: 10.1016/j.ultsonch.2019.03.023.
[141] M. Başlar, M. Kılıçlı, O.S. Toker, O. Sağdıç, M. Arici, Ultrasonic vacuum drying technique as a novel process for shortening the drying period for beef and chicken meats, Innovative Food Sci. Emerg. Technol. 26 (12) (2014) 182–190.
[142] M. Başlar, M. Kılıçlı, B. Yalınkılıç, Dehydration kinetics of salmon and trout fillets using ultrasonic vacuum drying as a novel technique, Ultrason. Sonochem. 27 (11) (2015) 495–502.
[143] Z. Chen, X. Guo, T. Wu, A novel dehydration technique for carrot slices implementing ultrasound and vacuum drying methods, Ultrason. Sonochem. 30 (5) (2016) 28–34.
[144] R.D.A. Amaral, I. Achaerandio, B.C. Benedetti, M. Pujolà, The influence of edible coatings, blanching and ultrasound treatments on quality attributes and shelf-life of vacuum packaged potato strips, LWT – Food Science and Technology 85 (B) (2017) 449–455.
[145] E.V.da.S. Júnior, L.L. de Melo, R.A.B. de Medeiros, Z.M.P. Barros, P.M. Azoubel, Influence of ultrasound and vacuum assisted drying on papaya quality parameters, LWT 97 (11) (2018) 317–322.
[146] S. Liu, W. Zhu, X. Bai, Effect of ultrasonic energy density on moisture transfer during ultrasound enhanced vacuum drying of honey, J. Food Meas. Charact. 13 (1) (2019) 559–570.
[147] E.S. da Silva, S.C.R. Brandao, A.L. da Silva, Ultrasound-assisted vacuum drying of nectarine, J. Food Eng. 246 (2019) 119–124.
[148] C. Brines, A. Mulet, J.V. García-Pérez, E. Riera, J.A. Cárcel, Influence of the ultrasonic power applied on freeze drying kinetics, Physics Procedia 70 (2015) 850–853.
[149] J. Ve, D. Santacatalina, J.A. Fissore, A. Cárcel, J.V. Mulet, García-Pérez, Model-based investigation into atmospheric freeze drying assisted by power ultrasound, J. Food Eng. 151 (4) (2015) 7–15.
[150] Md.N. Islam, M. Zhang, H. Liu, X. Cheng, Effects of ultrasound on glass transition temperature of freeze-dried pear (Pyrus pyrifolia) using DMA thermal analysis, Food Bioprod. Process. 94 (4) (2015) 229–238.
[151] D. Colucci, D. Fissore, C. Rossello, J.A. Carcel, On the effect of ultrasound-assisted atmospheric freeze-drying on the antioxidant properties of eggplant, Food Res. Int. 106 (4) (2018) 580–588.
[152] F. Ren, C.A. Perussello, Z. Zhang, J.P. Kerry, B.K. Tiwari, Impact of ultrasound and blanching on functional properties of hot-air dried and freeze dried onions, LWT 87 (1) (2018) 102–111.
[153] X. Cao, M. Zhang, A.S. Mujumdar, Q. Zhong, Z. Wang, Effects of ultrasonic pretreatments on quality, energy consumption and sterilization of barley grass in freeze drying, Ultrason. Sonochem. 40 (2) (2018) 333–340.
[154] Y. Cui, C.L. Xu, Q. Han, Effect of ultrasonic vibration on unmixed zone formation, Scr. Mater. 55 (11) (2006) 975–978.
[155] J. Wang, X. Hong, Research on Twin-arc TIG welding with ultrasonic excitation and its effect to weld, Key Eng. Mater. 450 (2011) 300–303.
[156] H. Dong, L. Yang, C. Dong, S. Kou, Improving arc joining of Al to steel and Al to stainless steel, Mater. Sci. Eng., A 534 (1) (2012) 424–435.
[157] B. Qi, M. Yang, B. Cong, F. Liu, The effect of arc behavior on weld geometry by high-frequency pulse GTAW process with 0Cr18Ni9Ti stainless steel, Int. J. Adv. Manufact. Technol. 66 (9) (2013) 1545–1553.
[158] Y.B. Zhong, C.S. Wu, G.K. Padhy, Effect of ultrasonic vibration on welding load, temperature and material flow in friction stir welding, J. Mater. Process. Technol. 239 (1) (2017) 273–283.
[159] S. Kumar, C.S. Wu, A novel technique to join Al and Mg alloys: Ultrasonic vibration assisted linear friction stir welding, Mater. Today:. Proc. 5 (2018) 18142–18151.
[160] A. Yousefpour, M. Hojjati, J.P. Immarigeon, Fusion bonding/welding of thermoplastic composites, J. Thermoplast. Compos. Mater. 17 (7) (2004) 303–341.
[161] M.P. Matheny, K.F. Graff, Ultrasonic welding of metals, in: J.A. Gallego-Juárez, K.F. Graff (Eds.), Power ultrasonics: applications of high-intensity ultrasound,

Woodhead Publishing, 2015, pp. 259–293.
[162] K. Wang, D. Shriver, Y. Li, M. Banu, S. Jack Hu, G. Xiao, J. Arinez, H.T. Fan, Characterization of weld attributes in ultrasonic welding of short carbon fiber reinforced thermoplastic composites, J. Manuf. Processes 29 (10) (2017) 124–132.
[163] T. Kondo, E. Kano, Effect of free radicals induced by ultrasonic cavitation on cell killing, Int. J. Radiat Biol. 54 (3) (1988) 475–486.
[164] Z. Pan, W. Qu, H. Ma, G.G. Atungulu, T.H. McHugh, Continuous and pulsed ultrasound-assisted extractions of antioxidants from pomegranate peel, Ultrason. Sonochem. 18 (5) (2011) 1249–1257.
[165] M.H. Ahmad-Qasem, J. Cánovas, E. Barrajón-Catalán, V. Micol, J.A. Cárcel, J.V. García-Pérez, Kinetic and compositional study of phenolic extraction from olive leaves (var. Serrana) by using power ultrasound, Innovative Food Sci. Emerg. Technol. 17 (2013) 120–129.
[166] S. Both, F. Chemat, J. Strube, Extraction of polyphenols from black tea–conventional and ultrasound assisted extraction, Ultrason. Sonochem. 21 (3) (2014) 1030–1034.
[167] S. Rodrigues, F.A. Fernandes, E.S. de Brito, A.D. Sousa, N. Narain, Ultrasound extraction of phenolics and anthocyanins from jabuticaba peel, Ind. Crops Prod. 69 (7) (2015) 400–407.
[168] M. Wang, B. Huang, C. Fan, K. Zhao, H. Hu, X. Xu, S. Pan, F. Liu, Characterization and functional properties of mango peel pectin extracted by ultrasound assisted citric acid, Int. J. Biol. Macromol. 91 (10) (2016) 794–803.
[169] L. Zhang, C. Zhou, B. Wang, A.E.A. Yagoub, H. Ma, X. Zhang, M. Wu, Study of ultrasonic cavitation during extraction of the peanut oil at varying frequencies, Ultrason. Sonochem. 37 (7) (2017) 106–113.
[170] I. Ayim, H. Ma, E.A. Alenyorege, Z. Ali, P.O. Donkor, Influence of ultrasound pretreatment on enzymolysis kinetics and thermodynamics of sodium hydroxide extracted proteins from tea residue, J. Food Sci. Technol. 55 (3) (2018) 1037–1046.
[171] C. Goltz, S. Ávila, J.B. Barbieri, L. Igarashi-Mafra, M.R. Mafra, Ultrasound-assisted extraction of phenolic compounds from Macela (Achyrolcine satureioides) extracts, Ind. Crops Prod. 115 (5) (2018) 227–234.
[172] R. Giri, G. Nath, P.K. Kar, Extraction of energy material: an ultrasonic approach, Mater. Today Proc. 5 (2018) 25591–25598.
[173] L. Santos-zea, M. Antunes-Ricardo, J.A. Gutierrez-Uuribe, J.V. García-Pérez, J. Benedito, Effect of ultrasound transducer design on the acoustically-assisted supercritical fluid extraction of antioxidants from oregano, Ultrason. Sonochem. 47 (10) (2018) 47–56.
[174] E.S. Dassoff, Y.O. Li, Mechanisms and effects of ultrasound-assisted supercritical CO2 extraction, Trends Food Sci. Technol. 86 (4) (2019) 492–501.
[175] H. Kiani, D.W. Sun, Z. Zhang, The effect of ultrasound irradiation on the convective heat transfer rate during immersion cooling of a stationary sphere, Ultrason. Sonochem. 19 (6) (2012) 1238–1245.
[176] N.E. Hotrum, P. de Jong, J.C. Akkerman, M.B. Fox, Pilot scale ultrasound enabled plate heat exchanger – Its design and potential to prevent biofouling, J. Food Eng. 153 (5) (2015) 81–88.
[177] Y. Chen, S. Sun, Y. Lai, C. Ma, Influence of ultrasound to convectional heat transfer with fouling of cooling water, Appl. Therm. Eng. 100 (5) (2016) 340–347.
[178] P. Gao, X. Zhou, B. Cheng, D. Zhang, G. Zhou, Study on heat and mass transfer of droplet cooling in ultrasound wave, Int. J. Heat Mass Transf. 107 (C) (2017) 916–924.
[179] O. Bulliard-Sauret, S. Ferrouillat, L. Vignal, A. Memponteil, N. Gondrexon, Heat transfer enhancement using 2 MHz ultrasound, Ultrason. – Sonochem. 39 (11) (2017) 262–271.
[180] T. Hou, Y. Chen, Z. Wang, C. Ma, Experimental study of fouling process and antifouling effect in convective heat transfer under ultrasonic treatment, Appl. Therm. Eng. 140 (7) (2018) 671–678.
[181] F. Liu, S. Chen, J. Lee, Feasibility study of heat transfer enhancement by ultrasonic vibration under subcooled pool condition, Heat Transfer Eng. 39 (7–8) (2018) 654–662.
[182] O. Bulliard-Sauret, J. Berindei, S. Ferrouillat, L. Vignal, A. Memponteil, C. Poncet, J.M. Leveque, N. Gondrexon, Heat transfer intensification by low or high frequency ultrasound: thermal and hydrodynamic phenomenological analysis, Exp. Therm Fluid Sci. 104 (6) (2019) 258–271.
[183] C. Bartoli, F. Baffigi, Effects of ultrasonic waves on the heat transfer enhancement in subcooled boiling, Exp. Therm Fluid Sci. 35 (3) (2011) 423–432.
[184] F. Baffigi, C. Bartoli, Influence of the ultrasounds on the heat transfer in single phase free convection and in saturated pool boiling, Exp. Therm Fluid Sci. 36 (1) (2012) 12–21.
[185] B. Li, X. Han, Z. Wan, X. Wang, Y. Tang, Influence of ultrasound on heat transfer of copper tubes with different surface characteristics in sub-cooled boiling, Appl. Therm. Eng. 92 (1) (2016) 93–103.
[186] A. Mosyak, G. Hetsroni, M. Fichman, L. Moldavsky, E. Pogrebnyak, Effect of heater size on ultrasonic enhancement of boiling in water and surfactant solutions, Int. J. Multiph. Flow 79 (3) (2016) 181–189.
[187] M. Zheng, B. Li, Z. Wan, B. Wu, Y. Tang, J. Li, Ultrasonic heat transfer enhancement on different structural tubes in LiBr solution, Appl. Therm. Eng. 106 (8) (2016) 625–633.
[188] Z. Wang, Y. Xu, F. Su, Y. Wang, A light lithium niobate transducer for the ultrasonic de-icing of wind turbine blades, Renewable Energy 99 (12) (2016) 1299–1305.
[189] C. Yin, Z. Zhang, Z. Wang, Numerical simulation and experimental validation of ultrasonic de-icing system for wind turbine blade, Appl. Acoust. 114 (12) (2016) 19–26.
[190] J. Zeng, B. Song, Research on experiment and numerical simulation of ultrasonic de-icing for wind turbine blades, Renew. Energy 113 (6) (2017) 706–712.
[191] Y. Wang, Y. Xu, Q. Huang, Progress on ultrasonic guided waves de-icing techniques in improving aviation energy efficiency, Renew. Sustain. Energy Rev. 79 (11) (2017) 638–645.
[192] Y. Wang, Y. Xu, Y. Lei, An effect assessment and prediction method of ultrasonic de-icing for composite wind turbine blades, Renew. Energy 118 (4) (2018) 1015–1023.
[193] Z. Wang, Y. Xu, Y. Gu, Lithium niobate ultrasonic transducer design for Enhanced Oil Recovery, Ultrason. Sonochem. 27 (11) (2015) 171–177.
[194] Z. Wang, Y. Xu, The development of recent high-power ultrasonic transducers for Near-well ultrasonic processing technology, Ultrason. Sonochem. 37 (7) (2017) 536–541.
[195] Z. Wang, C. Yin, Reprint of: State-of-the-art on ultrasonic oil production technique for EOR in China, Ultrason. Sonochem. 40 (1) (2018) 201–207.
[196] X. Huang, C. Zhou, Q. Suo, L. Zhang, S. Wang, Experimental study on viscosity reduction for residual oil by ultrasonic, Ultrason. Sonochem. 41 (3) (2018) 661–669.
[197] A. Qi, L.Y. Yeo, J.R. Friend, Interfacial destabilization and atomization driven by surface acoustic waves, Phys. Fluids 20 (7) (2008) 074103.
[198] D.J. Collins, O. Manor, A. Winkler, H. Schmidt, J.R. Friend, L.Y. Yeo, Atomization off thin water films generated by high-frequency substrate wave vibrations, Phys. Rev. 86 (5) (2012) 056312.
[199] K.A. Ramisetty, A.B. Pandit, P.R. Gogate, Investigations into ultrasound induced atomization, Ultrason. Sonochem. 20 (1) (2013) 254–264.
[200] P. Deepu, C. Peng, S. Moghaddam, Dynamics of ultrasonic atomization of droplets, Exp. Therm Fluid Sci. 92 (4) (2018) 243–247.
[201] K. Raafat, W. Samy, Phytochemical and biological evaluation of ultrasound-assisted spray dried lonicera etrusca for potential management of diabetes, Rec. Nat. Prod. 12 (4) (2018) 367–379.
[202] S. Aghamohammadi, M. Haghighi, A. Ebrahimi, Pathways in particle assembly by ultrasound-assisted spray-drying of kaolin/SAPO-34 as a fluidized bed catalyst for methanol to light olefins, Ultrason. Sonochem. 53 (5) (2019) 237–251.
[203] H. Liu, W. Chang, C. Chou, B. Pan, C. Liu, Controllable electrochromic polyamide film and device produced by facile ultrasonic spray-coating, Scient. Rep. (Nat. Publisher Group) 7 (9) (2017) 1–10.
[204] J. Huang, Y. Hsueh, Y. Zhang, Silver nanowire doped active carbon thin film electrode by ultrasonic spray coating for high performance supercapacitor, Surf. Coat. Technol. 350 (9) (2018) 788–794.
[205] X. Meng, W. de Jong, T. Kudra, A state-of-the-art review of pulse combustion: principles, modeling, applications and R&D issues, Renew. Sustain. Energy Rev. 55 (3) (2016) 73–114.
[206] Y. Zhu, Y. Lu, B. Gao, D. Wang, G. Yang, C. Guo, Ultrasonic-assisted emulsion synthesis of well-distributed spherical composite CL-20@PNA with enhanced high sensitivity, Mater. Lett. 205 (10) (2017) 94–97.
[207] D.D. Nguyen, H.H. Ngo, Y.S. Yoon, A new approach involving a multi transducer ultrasonic system for cleaning turbine engines' oil filters under practical conditions, Ultrasonics 71 (9) (2016) 256–263.
[208] J. Choi, T.H. Kim, H.Y. Kim, w. Kim, Ultrasonic washing of textiles, Ultrason. Sonochem. 29 (3) (2016) 563–567.
[209] H. Lais, P.S. Lowe, T.H. Gan, Numerical modelling of acoustic pressure fields to optimize the ultrasonic cleaning technique for cylinders, Ultrason.-Sonochem. 45 (7) (2018) 7–16.
[210] A. Milcamps, A.V. Dommelen, J. Stigter, J. Vanderleyden, F.J.D. Bruijn, Influence of acoustic waves on deposition and coagulation of fine particles, Int. J. Environ. Res. 7 (1) (2013) 131–138.
[211] W.T. Yuen, S.C. Fu, The use of nonlinear acoustics as an energy-efficient technique for aerosol removal, Aerosol Sci. Technol. 48 (9) (2014) 907–915.
[212] J.Z. Liu, J. Wang, G.X. Zhang, J.H. Zhou, K.F. Cen, Frequency comparative study of coal-fired fly ash acoustic agglomeration, J. Environ. Sci. 23 (11) (2011) 1845–1851.
[213] D. Zhou, Z. Luo, J. Jiang, H. Chen, M. Lu, M. Fang, Experimental study on improving the efficiency of dust removers by using acoustic agglomeration as pretreatment, Powder Technol. 289 (2) (2016) 52–59.
[214] J. Yan, L. Chen, Z. Li, Removal of fine particles from coal combustion in the combined effect of acoustic agglomeration and seed droplets with wetting agent, Fuel 165 (2) (2016) 316–323.
[215] J. Yan, Q. Lin, S. Zhao, Effect of seed nuclei combined with acoustic field on fine particles removal, Power Technol. 340 (12) (2018) 8–16.